Sculpture Surface Machining

by

Birhan Ufku Guzel

A Thesis Submitted to the
Graduate School of Engineering
in Partial Fulfillment of the Requirements for
the Degree of

Master of Science

in

Industrial Engineering

Koc University

June 2003

Koc University

Graduate School of Sciences and Engineering

This is to certify that I have examined this copy of a master's thesis by

Birhan Ufku Guzel

and have found that it is complete and satisfactory in all respects,

and that any and all revisions required by the final

examining committee have been made.

Committee Members:

____

Ismail Lazoglu, Ph. D. (Advisor)

____

Erhan Budak, Ph. D.

____

Selcuk Savas, Ph. D.

Date: ________________________

ABSTRACT

The ball end milling process is used extensively in machining of sculpture surfaces in automobile, die/mold and aerospace industries. In planning machine operations, the process planner has to be conservative in selecting machining conditions with respect to metal removal rate in order to avoid unwanted results such as chipping, cutter breakage or overcut due to excessive cutter deflection. These problems are particularly important for machining of sculptured surfaces where axial and radial depths of cut are abruptly changing. For this reason it will be very critical to provide the process planner with guidance in selecting machining conditions. One solution to this problem is to consider the cutting force in the stage of selecting machining conditions. If the process planner can predict the cutting force for a certain machining condition, it would be very helpful in judging whether the selected condition is appropriate. As a result, a mathematical model is developed in this work for the prediction of cutting force system in ball end milling of sculpture surfaces. The model has the ability to calculate the workpiece/cutter intersection domain automatically for a given cutter path, cutter and workpiece geometries. In addition to predicting the cutting forces, the model also determines the surface topography and scallop height variations along the workpiece surface which can be visualized in solid form. Extensive experiments are performed to validate the theoretical model with measured forces and surface topography outputs. Even for complex part geometries, the mathematical model predictions agree well with experimental measurements.

ACKNOWLEDGEMENTS

I would like to acknowledge gentle efforts of the people in GYTE for CMM measurements, Levent Demirel for his help in taking magnified photographs of the cutters, my friends in the office for their patience, my advisor Ismail Lazoglu and my family for their unique support in completion of this thesis.

TABLE OF CONTENTS

LIST OF TABLES

LIST OF FIGURES

NOMENCLATURE

a	axial depth of cut
r	tool radius in x-y plane at a point defined by ψ
t_x	feed per tooth
t_c	instantaneous chip thickness
i_0	helix angle at ball shaped flute and shank meeting point
β	lag angle between the tangent line at the tip of the flute and axial location z
θ	cutting element rotation angle
$\Delta\theta$	discrete cutting element rotation angle
ψ	cutting element position angle
R_b	ball radius
N_f	number of flutes
ω	spindle speed in revolution per minute
F_r, F_ψ, F_t	cutting forces in tangential, radial and axial directions
dF_X, dF_Y, dF_Z	differential cutting forces in x, y, and z directions
K_{rc}, $K_{\psi c}$, K_{tc}	tangential, radial and axial cutting force coefficients in milling
K_{re}, $K_{\psi e}$, K_{te}	tangential, radial and axial edge force coefficients in milling
$(dz)_{kn}$	differential height along the longitudinal cutter axis at the k^{th} discrete point on the nth flute
Ω	rotation angle of flute
φ_p	cutter pitch angle
n	flute number
β_k	lag angle between the k^{th} discrete point on cutting edge and the cutter tip
dA_c	differential chip load
$P(f)$	constant pressure applied on the workpiece as a function of feedrate
f_s	data sampling frequency

Chapter 1

INTRODUCTION

Precision and economical manufacturing of a part is a popular subject about which people from different disciplines have performed numerous studies. Although industrial engineering aspects, such as the scheduling of parts and economics, also play an important role in cost effective manufacturing, this study focuses only on the physical principles of machining, mainly on a certain type of metal cutting operations.

Metal cutting is one of the most widely used manufacturing processes to produce final shape of products, and its technology continues to advance in parallel with developments in materials, computers and sensors. A blank is converted into a final product by cutting extra material away by turning, drilling, milling, broaching, boring and grinding operations conducted on Computer Numerically Controlled (CNC) tools.

Metal cutting operations take place between a cutting tool and workpiece material mounted on a machine tool. The motion of the machine tool is controlled by its CNC unit, and the Numerically Controlled (NC) commands to CNC are generated on computer-aided design/computer-aided manufacturing (CAD/CAM) systems. The productivity and accuracy of the metal removal operation depend on the preparation of NC programs, planning of machining process parameters and cutting conditions, cutter geometry, work and tool materials, machine tool rigidity, and performance of the CNC unit.

The milling operation, which is the subject under investigation in this study, is an intermittent cutting process, commonly using a multi-flute cutter. A milling cutter is held in a rotating spindle, while the workpiece clamped on the table is linearly moved toward the cutter. Each milling tooth therefore traces a trochoidal path, producing varying but periodic chip thickness at each tooth passing interval. Depending on the workpiece geometry, different milling cutters and machines are used [1].

The ball end milling process is used extensively in the machining of free-form surfaces in die/mold and aerospace industries. However, since its cutting geometry is often changing, it is somewhat difficult to achieve high quality and productive machining. Therefore, in planning machine operations, the part programmer has to be conservative most of the time, in selecting machining conditions with respect to metal removal rate in order to avoid undesirable results such as chipping, cutter breakage or overcut due to excessive cutter deflection. These problems are particularly important for the machining of sculptured surfaces where axial and radial depths of cut are abruptly changing. One solution to this problem is to consider the cutting force in the stage of selecting machining conditions. If the process planner can predict the cutting force for a certain machining condition, it would be very helpful in judging whether the selected condition is appropriate [2]. Besides, knowledge on the cutting forces helps to design better fixtures, contributing to an increase in surface qualities of parts. Moreover a cutting force model for sculpture surfaces can be utilized in model based process control and monitoring algorithms in ball-end milling process [3].

In this study, a comprehensive cutting force model has been developed which employs a Boolean approach. For given cutter/workpiece geometry, process parameters and tool path, the model determines the surface topography with scallop height variations along the workpiece surface which can also be visualized in 3D.

Chapter 2 provides necessary background and literature review on milling analysis. The fundamentals of metal cutting analysis, cutting mechanics and previous models for prediction of cutting forces in ball-end milling are reviewed.

Chapter 3 describes the tool geometry and cutting edge representation in the system together with the cutter/workpiece intersection model; the mechanism underlying the 3D visualization of the system is explained. Thereafter modeling of ball-end milling forces is explained, including the chip load model and the cutting force model.

Calibration process details are given in Chapter 4, where the methodology that is employed to determine the cutting constants for the force model is described. In addition to that, the proposed methodology for more accurate prediction of the cutting force in Z direction is explained in detail.

Validation tests under various conditions are described and their results given in Chapter 5, together with the discussion of these results.

The thesis is concluded with a short summary of the performed study and future research work.

Chapter 2

LITERATURE REVIEW

2.1 Overview

Milling is used extensively in the manufacturing industry where both precision and efficiency are critical. In this process, the component shape, size and its surface finish is generated by systematically removing the excess material from the original workpiece by a cutting tool. The milling cutter has a number of cutting edges. The workpiece is gradually fed to the rotating cutter during milling. Chips are removed by each cutting edge during revolution and a surface is produced. Milling is one of the most important manufacturing processes because it can produce a wide variety of component shapes and sizes with high dimensional accuracy and good surface finish. Besides milling can be computer controlled and automated through use of CNC machine tools. In many of these operations the cutting force is an important parameter either with respect to the deflection (dimensional tolerance), breakage of the cutter and the stability of the process. Moreover, knowledge of the magnitude and variation of the cutting force with respect to the cutting conditions is essential for the process planning of milling operations. In addition to that a cutting force model for sculpture surfaces can be utilized in model based process control and monitoring algorithms in ball-end milling process [4].

The mechanics of milling can be best understood by examining the chip formation during the process. An early detailed kinematic analysis by Martelotti [5] showed that, due to the combined rotational and linear feeding motions of the cutter towards the workpiece, the true path of a cutter tooth is an arc of a trochoid, rather than a circle, which complicates the mathematics in the analysis. However, Martelotti claimed that, in most practical cutting conditions where the cutter radius is much larger than the feed per tooth, the circular tool path assumption is valid and the error introduced is insignificant. As the cutter rotates, the immersion angle (θ) varies, hence the chip load changes sinusoidally and given by Martelotti as:

$$t_c = t_x \cdot \sin(\theta) \tag{2.1}$$

where t_c is the instantaneous chip load, t_x is the feed per tooth and θ is the immersion angle of cutting point.

2.2 Milling Force Models

An early analysis of milling forces produced by a helical flute was presented by Koenigsberger et al. [6]. They related the elemental chip loading to rigid cutting forces through experimentally calibrated milling force coefficients K_t and K_r, in tangential and radial directions respectively. In general, these coefficients are identified through empirical curve fitting technique and provide little physical insight in terms of the nature of the process. The cutting forces were expressed as a function of cutting pressure exerted on the instantaneous chip area:

$$\begin{aligned} F_t &= K_t \cdot a \cdot t_x \cdot \sin(\theta) \\ F_r &= K_r \cdot F_t \end{aligned} \tag{2.2}$$

where a is the axial depth of cut, F_t and F_r are the cutting forces in tangential and radial directions respectively.

Other researchers employed the same model with improvements such as including the effect of runout and tool deflections [7, 8]. Tlusty and MacNeil [9], Armarego and Budak et al. [10] further improved the accuracy in predicting the milling force coefficients for cylindrical helical end mills by introducing an edge force component to their model.

While plenty of work has been done related to the mathematical models of flat end milling processes, those of ball end milling processes were developed only recently due to the complexity of the geometry. The mechanistic approach had limitations on milling with complex cutters such as ball-end mills which have variable geometry in the axial direction. As a result, Lim and Feng [11, 12] approximated the cutting force coefficients with a third degree polynomial which depends on the axial depth of cut. They then estimated the coefficients by iteratively curve fitting using average runout values on the cutters. Similarly, Yucesan and Altintas [13] presented a semi-mechanistic model which predicts the shear and friction load distribution on the rake and flake faces of the helical ball-end mill flutes. They used a complex mathematical model and identified the milling force coefficients through an empirical curve fit to measure average milling forces.

With the mechanistic model, prior evaluation of the milling force coefficients is necessary for any analysis and prediction. Milling calibration tests are required to be run at different feedrates, cutting speeds, and constant cutting geometry, and the results are applicable to a particular workpiece material-cutter pair only. However, the model allows a quick calibration of existing cutters and may turn out to be a practical and useful approach even in the case of complex cutters such as the ball-end mill if an appropriate methodology is applied.

As an alternative to the mechanistic approach, mechanics of milling has been studied to make use of the orthogonal cutting parameters for cutters with well defined geometry (without grooves, chip breakers, etc.), thus eliminating the need for new calibration tests each time the cutter geometry changes. Armarego [10, 14] was among a few researchers to apply the orthogonal to oblique transformations on milling force predictions. The basic idea is to represent the milling geometry by segments of oblique cutting processes. By measuring the forces in turning, Budak, Altintas and Armarego [15] identified the traditional material properties such as shear flow stress and friction angle from a set of standard orthogonal turning tests. They showed an accurate method of transformation between the orthogonal cutting parameters (i.e. shear stress, shear and friction angles) and local milling force coefficients, taking into consideration the cutter geometry such as helix angle and rake angle. Yang and Park [16] took a similar approach and applied the orthogonal theory on ball-end mills. They obtained the fundamental cutting parameters from orthogonal turning tests and simplified the analysis by approximating the oblique cutting on each ball-end flute by infinitesimal orthogonal processes. Later they considered the variation in the chip loads due to static tool deflections. Tai and Fuh [17] used a similar cutting model but they represented the cutting edge geometry as intersections between skew planes and spherical ball-end mill surface. Lazoglu and Liang [18] established a closed-form model for ball-end milling cutting force system in the frequency domain using an angular convolution technique, and analytical time domain predictions were obtained via inverse Fourier transformation of the cutting force frequency spectrums.

A cutting system is often subjected to some type of external dynamic forces. This forcing function can be time-dependent, harmonic, periodic, or random in nature. In dynamic milling, under some conditions, force induced vibrations may be inherent into the process, at the tooth passing frequency. For other conditions, the vibration may cause the cutting process to vary so that it supplies a positive input of energy to maintain the vibration, which is known as self induced or self-excited vibration in machining. Chatter is a self-excited type of vibration which occurs in metal cutting due to the lack of stiffness in the process, or can be best explained by a phenomenon called 'regeneration of waviness'. 'Regeneration of waviness' is a mechanism by which the input force is modulated by system dynamics so as to produce force variations and vibration. Chatter vibrations occur around the natural frequency of the most flexible part of the machine cutter/workpiece structure which is closest to the cutting point [4].

Tobias [19] and Tlusty [20] were among the few early researchers to study dynamic cutting. They explained the fundamental mechanism of chatter during turning and derived the stability theory which analytically predicts chatter free cutting conditions. Their theory was based on the orthogonal cutting model where the directions of cutting forces and the structural dynamics of the cutter/workpiece system were assumed constant. Chatter in milling, however, is different from turning in which the cutter rotates with respect to the structure/workpiece system. Sridhar [21] presented a milling stability model which requires numerical solution of the milling equation. Later Minis [22] proposed an improved method of solving the stability equation analytically by iteration. Budak et al. [23] have solved the chatter stability in milling for helical end mills by representing the time varying milling force coefficients in Fourier series, hence they were able to solve the stability equation analytically and more efficiently, taking into account the change in the milling force directions. Altintas and Lee [24] applied their theory to ball-end mills as well. Abrari and Elbestawi [25] also made a dynamic force model and a stability analysis for ball-end milling. They used the method of regenerative chip load calculation which accounts for the effects of both the surface undulations and the instantaneous deflection.

Recently, following the substantial improvement in computational power which is inexpensive to obtain and operate, numerical approaches are getting even more appealing for the researcher. Z-mapping is such an approach used by various authors including Kim et al. [26] or Lazoglu [3]. Lazoglu employed a Boolean approach in the model and in addition to predicting the cutting forces, the model determined the resulting surface topography and scallop height variations along the workpiece for given cutter/workpiece geometries and CL file. Kim estimated the cutter deflection and form error in a recent work [27], building upon his force prediction model. Ikua et al. [28, 29] constructed a model for prediction of cutting forces and machining error in ball-end milling of curved surfaces, investigating various cutting conditions. Jung et al. [30] suggested the exact chip engagement (ECES) method in order to calculate the chip thickness distribution along the cutting edge when the cutting velocity is not significantly large compared with the cutter feed. Shatla and Altan [31] developed a force model both for drilling and ball-end milling which also predicted temperatures on the flank side of the cutter. Bouzakis et al. [32] developed a milling simulation algorithm predicting the surface topography, cutting forces and the surface roughness.

Most of the models mentioned here are applicable to either machining of simple and limited workpiece geometries, such as 2½ axis milling cases, or can not detect the cutter/workpiece engagements regions automatically and can not simulate multi-pass machining operations. Even the more comprehensive, recent models do not consider the ball-end mill moving in a completely ‘free’ fashion in order to create free form surfaces. The idea of defining a practical mechanistic methodology that is widely applicable to all forms of machining with ball-end mills through utilization of previously proposed methods has been the motivation in this study.

Chapter 3

CUTTER/WORKPIECE GEOMETRY AND CUTTING FORCE MODEL

3.1 Introduction

A large variety of milling tools are available and used in die and mold manufacturing. Each cutting edge on the tool is carefully designed to ensure maximum cutting performance while minimizing the resulting cutting forces. A detailed analysis of the cutting edge geometry is also necessary for the development of the force model. In order to form the model, all of the acting components in cutting must be represented mathematically first, and thereafter, the relationships between these components in the real process must be defined building upon these representations.

In this chapter, the nature of the cutting tool has been given initially together with the determination of tool geometry where cutting edge is represented as a function of r, the vertical distance from a cutting point to the axis of cutter. This is followed by the methodology to determine the cutter/workpiece intersection regions in the model. The Matlab environment that is used to create the cutting components in 3D solid form is explained in detail.

Thereafter, a detailed description of the proposed force model is given. The utilized chip load model is introduced first, which is followed by the explanation of the mechanistic force model.

3.2 Tool Geometry

The important characteristics of milling tools are the macro geometry (cylindrical, ball-end, bull-nose, tapered ball-end mills, etc.), the micro geometry (helix angle, rake angle, relief angle, ball radius, etc.), the cutting material (e.g. carbide, HSS and PCBN), and coating material (e.g. TiN, TiALN).

In general, several aspects are considered concerning the cutting edge geometry:

- A positive rake angle improves the shearing and cutting actions and decreases the forces, but weakens the cutting edge and makes it more susceptible to wear and breakage.

- High helix angle "smoothens" and reduces the impact force during entry cutting.

- Presence of clearance angle reduces the rubbing on the machine surface thus improves the surface finish, but at the expense of weakening the cutting edge and more important, reducing process damping and increasing the likelihood of chatter vibrations. A second clearance angle may be provided to reduce the amount of grinding during sharpening.

Figure 3.1.a shows the common nomenclature for a helical end mill with N_f teeth. Each flute is inclined at a constant helix angle i_0 and the immersion angle for flute n changes along the axial direction. For cylindrical cutters which have a constant radius and helix angle, the immersion angle varies linearly with the height. At the height of z, the angular position θ of a cutting point on flute n can be described as:

$$\theta(z) = \Omega + (n-1)\cdot\phi_p - \frac{z}{R_b}\cdot\tan i_0 \tag{3.1}$$

where R_b is the cutter radius, $\phi_p = 2\pi / N_f$ is the cutter pitch angle. Ω is the base angle of the reference flute in global coordinate system.

As opposed to the straight-end mill, ball-end mill cutting edge geometry varies locally in the ball part. The varying radius r directly affects the cutting forces through its effect on the cutting velocity (Figure 3.1.b). With end mills, however, the material is always cutting at the periphery of the cutter at a constant speed.

The detailed geometry of a helical ball-end mill cutter is shown in Figure 3.2. Each flute lies on the surface of the hemisphere, and is ground with a constant helix lead. The flutes have a helix angle of i_0 at the ball-shank meeting boundary (Figure 3.1.b). Due to the reduction of radius at x-y planes towards the ball tip in axial z direction, the local helix angle for a discrete point along the cutting flute varies for constant helix-lead cutters.

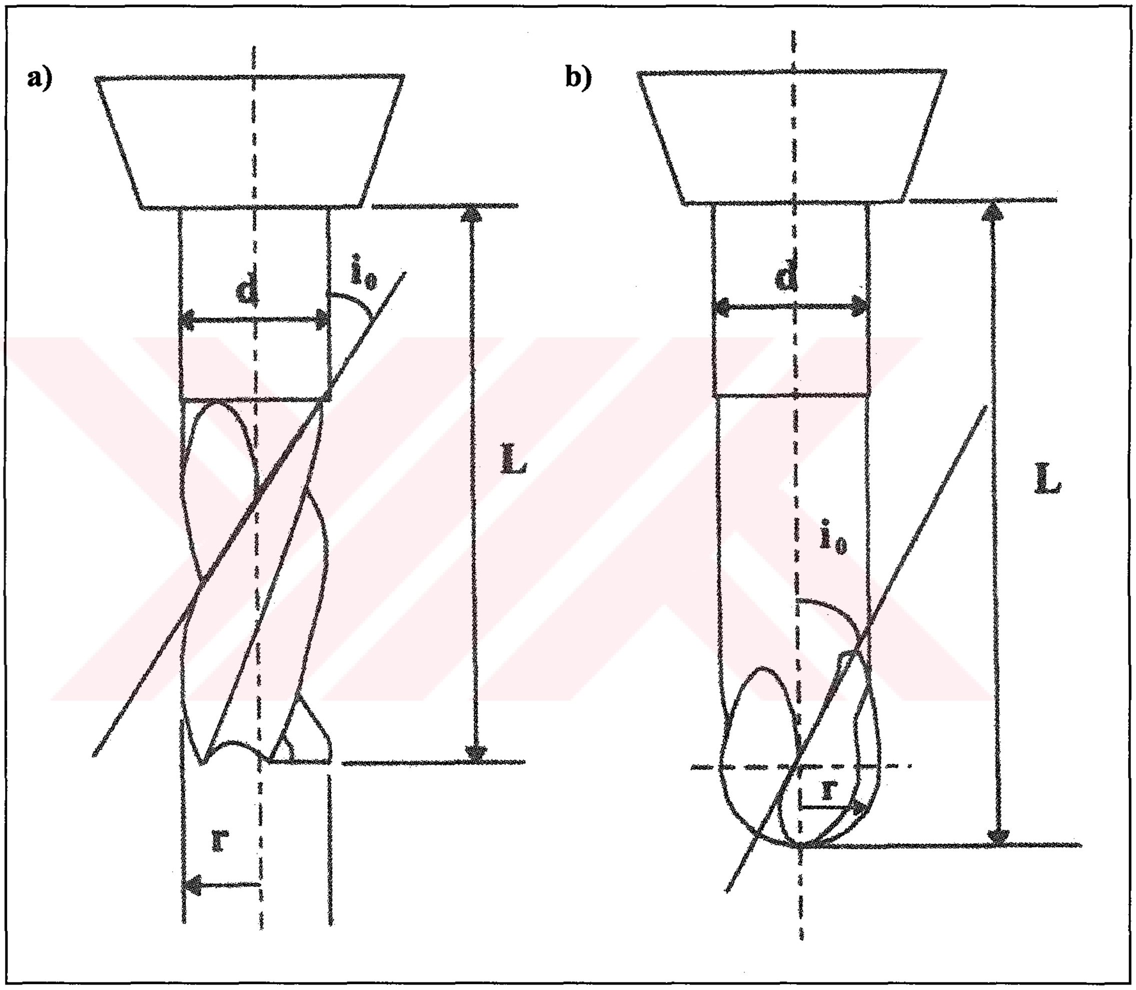

Figure 3.1: Macro geometries of;
a) Straight-end mill, b) Ball-end mill

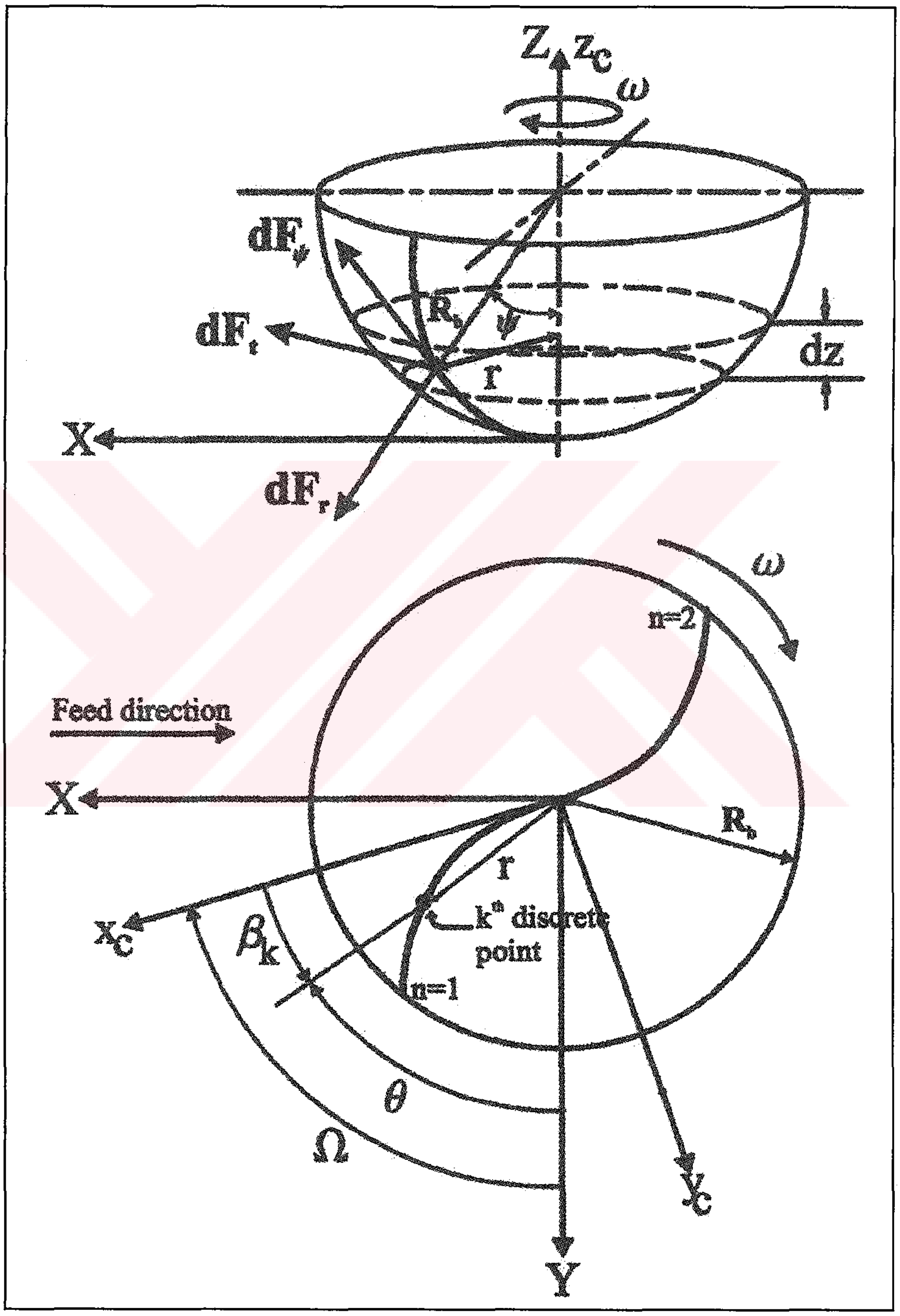

Figure 3.2: Illustration of the cutting force components and angular relationships

The expression for the shape of the ball part is given by,

$$x^2 + y^2 + (R_b - z)^2 = R_b^2 \tag{3.2}$$

where R_b is the ball radius of the cutter measured from the center of the sphere part. The cutter radius r in x-y plane at axial location z is,

$$r^2 = x^2 + y^2 \tag{3.3}$$

and is zero at the ball tip. The z coordinate of a point located on the cutting edge is,

$$z = \frac{R_b \beta_k}{\tan i_0} \tag{3.4}$$

where β_k, which exists due to the helix angle, is the lag angle between the tangent line (x_c) at the tip of the flute at ($z=0$) and axial location z (See Fig 3.2).

There are two ways to represent cutting edge geometries of a cutter in the model;

-An explicit mathematical representation of the cutting edge supplied by the cutter manufacturer may exist: In this case, cutting edge formulation can be easily transformed into three orthogonal cutter axes, namely x_c- y_c- z_c. The x_c axis is tangent to the cutting edge at the tip of the cutter, z_c is the axis along the cutter longitudinal axis (starting from the tip), y_c is the third orthogonal axis.

-Representation of the cutting edge via polynomial fitting to CMM data set: For the representation of the cutting edge geometry, the cutting edge coordinates can be measured using a coordinate measurement machine (CMM) with a rotary table. Alternatively, the measurements can be made from a sufficiently magnified picture of the cutting edge. After collection of the data points on the cutting edges, polynomial fitting can be performed on this data.

In the model, since the explicit mathematical representation of the cutting edge was not supplied by the cutter manufacturer, representation by polynomial fitting to a measured set of points has been made. For this purpose a magnified view of the cutter (with 12 mm diameter, two-flute carbide ball-end mill, CoroMill Plura series from Sandvik) has been obtained using a precise-zooming camera as seen in Figure 3.3. A cutting edge of the cutter has been divided into grids. 20 distinct points have been taken on the cutting edge to resemble the cutting edge (Figure 3.4). The relative locations of these points have been entered to Matlab to obtain a third degree fitted polynomial that formed the cutting edge geometry for the mathematical model. The following equation has been obtained for β;

$$\beta = 0.0036 \cdot r^3 - 0.0205 \cdot r^2 + 0.0547 \cdot r - 0.041 \qquad (3.5)$$

where r is the radius (in [mm]) of a point on the cutting edge on a plane perpendicular to the cutter longitudinal axis, and β is the angle (in [radian]) between the line which connects this point to the tip and the line which is tangent to the cutting edge at the tip (Figure 3.5).

The cutting edge geometry can be represented in the cutter coordinate system as the following;

$$x_c = r \cdot \cos(\beta), \quad y_c = r \cdot \sin(\beta), \quad z_c = R_b - \sqrt{R_b^2 - r^2} \qquad (3.6)$$

Therefore, by varying r value from the tip to cutter ball radius (i.e., 0-R_b), the full cutting edge profile can be determined from these equations.

3.3 Cutter/Workpiece Intersection Model

Determining the cutter/workpiece engagement is very critical, since it affects the chip load and cutting force calculations directly. The purpose of using a cutter/workpiece intersection model is to determine which part of the cutter is engaged with the workpiece at any instant of machining time.

The cutter and workpiece are meshed into small elements whose projection into the *x-y* plane is square. Workspace and workpiece are also meshed into the same size elements (Figure 3.6). Size selection of the grids is important in the sense that the smaller the mesh size, the longer the simulation time, and the better the accuracy of the predictions. In order to obtain this meshed structure in Matlab, a two dimensional matrix is utilized. The number of rows and columns in the matrix determined the width and length of the workpiece, respectively. Each element of the matrix structure kept the height

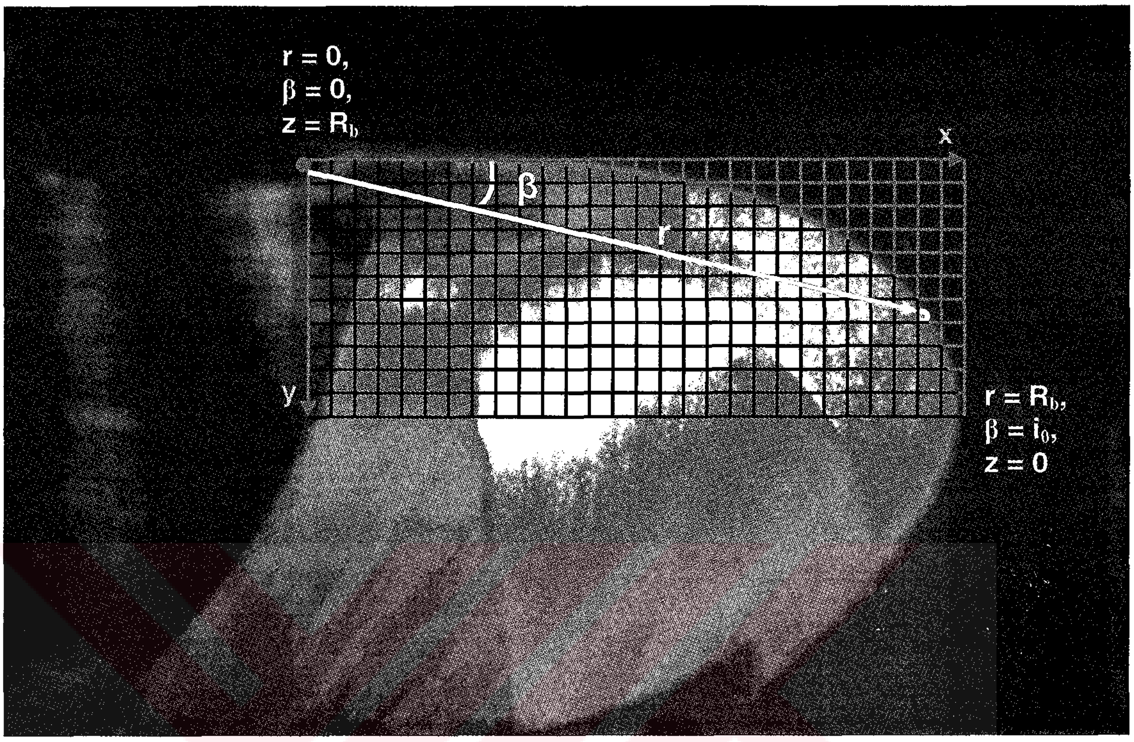

Figure 3.3: Ø12mm carbide ball-end mill cutter (view from the tip - 20 times magnified).

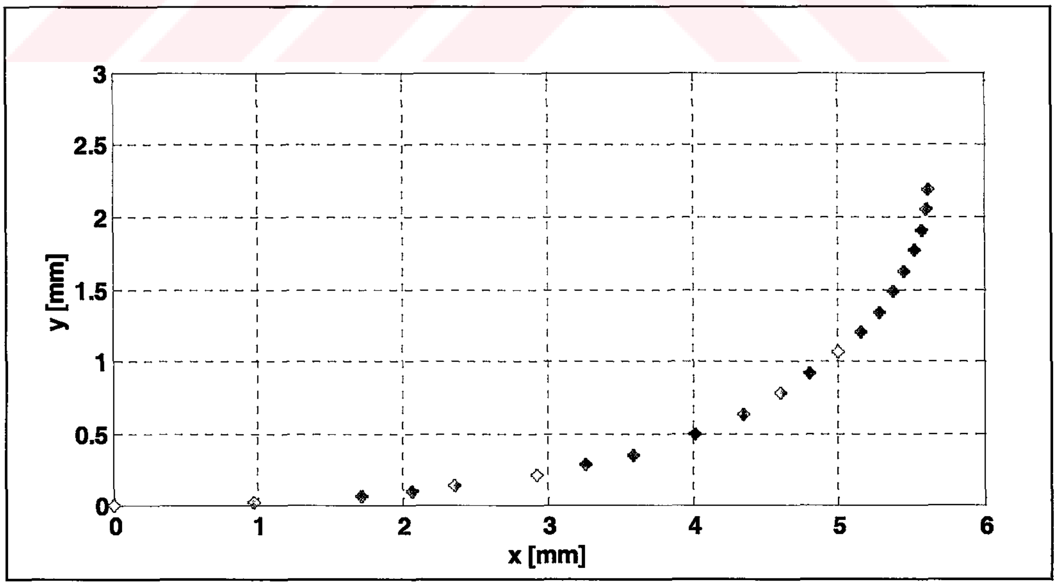

Figure 3.4: Measured data points for the cutting edge (x-y view).

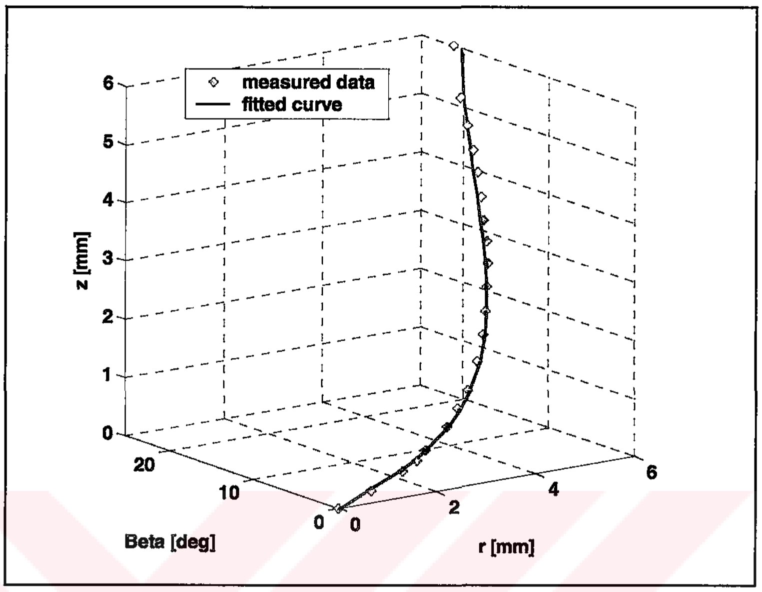

Figure 3.5: Third degree polynomial fit obtained for $\beta(r)$.

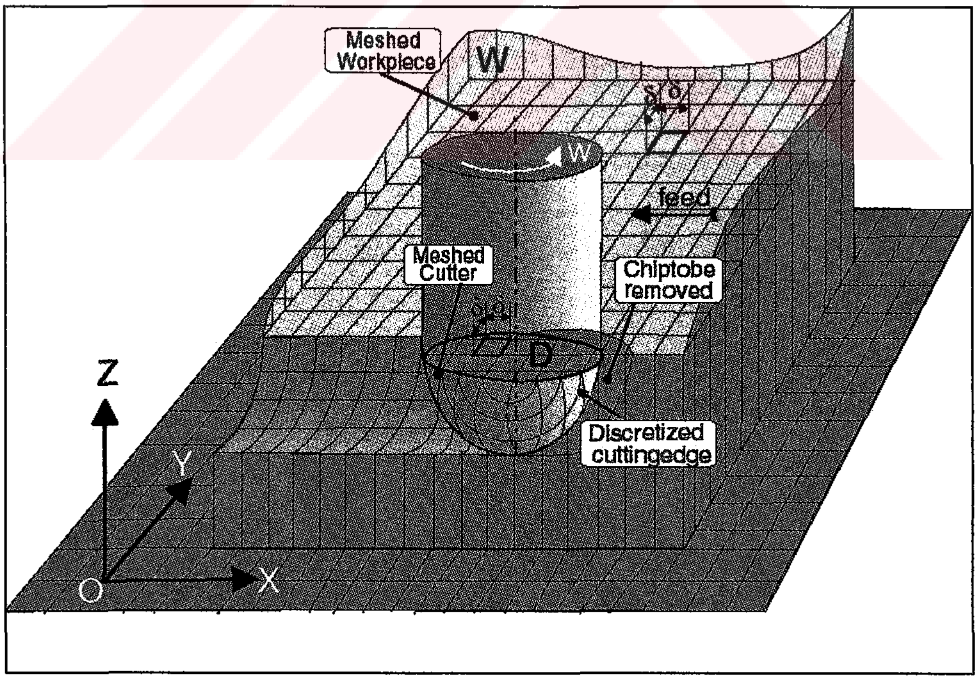

Figure 3.6: Illustration of meshed workpiece and cutter

of the workpiece at the corresponding spot in reality. The cutter is also created as a two dimensional matrix in the Matlab environment. As different from the workpiece matrix, the values of the elements of the cutter matrix have values only in the region where cutter is actually standing (i.e. the only place cutting may occur). The cutter is resembled as a half sphere connected to a cylinder in the model. In order to arrange the size selection of the grids, the number of rows and columns of the two dimensional matrix structures are changed. As the matrices grow in size the accuracy of the model increases naturally, however the simulation time significantly increases as well.

Based on the inputs of the model (tool path, cutter and workpiece geometry), the cutter is translated and rotated at the nodal points of the mesh elements in the workspace according to the tool and workpiece kinematics. Considering spindle speed and feedrate together with the other inputs, all the locations of discrete points for each region of the ball-end mill during the machining process are calculated in terms of X-Y-Z global coordinates (Figure 3.6). Thereafter, the instantaneous workpiece heights at each of the *x-y* coordinates of the cutting region are also determined, and based on the difference between the cutter and workpiece height at these points, the algorithm determines which portion of the cutter is in contact with the workpiece. This can also be explained as the following; let D and W be defined as the cutter domain and workpiece surface at any instant of machining, respectively (Figure 3.6) and let $P(X_d, Y_d, Z_d)$ be a discrete point on the cutting nose, $Q(X_w, Y_w, Z_w)$ be a nodal point on the workpiece surface. If and only if at any time, the condition,

$$\{Z_d \leq Z_w \mid P \in D, Q \in W, X_d = X_w, Y_d = Y_w\} \tag{3.7}$$

is satisfied then the point P is said to be in cutting with point Q and considered to be in the engagement domain at that instant. In terms of matrices, of course, values of the heights in cutter matrix and workpiece matrix structures are updated at any instant of the simulation. If the height value of a workpiece element is higher than that of the corresponding cutter element, the workpiece element is decreased to cutter level first and thereafter the spot is marked to be in the engagement domain.

In the next increment, the cutter tip travels according to toolpath, and the workpiece height at this $Q(X_w, Y_w, Z_w)$ is set to the Z_d on the workpiece mesh matrix. The simulation keeps and updates the workpiece geometry after each cut. This procedure makes it possible to visualize the surface topography at every instant of machining and scallop heights on the machined surface in 3D at the end of the simulation. A sample of machined workpiece simulation output is provided in Figure 3.7.a and Figure 3.7.b together with the generated engagement regions during a convex cut.

3.4 Modeling of Milling Forces

3.4.1 Introduction

In the machining of complex and costly parts such as those involved in aircraft or die and mold industries and mainly the sculpture surfaces, prior knowledge of the milling forces, surface form errors and chatter vibrations is essential to assist engineers in designing machine tools, jigs and fixtures. It can also help them in selecting appropriate cutting conditions to reduce tool deflection and chatter vibrations which affect the surface quality of the finished parts. For instance, if the chip load is selected to be too large, the forces cause chipping of the cutting edge or even tool breakage, while a small chip load will decrease productivity. Additionally a cutting force model for sculpture surfaces can be utilized in model based process control and monitoring algorithms in ball-end milling process.

Many recent investigations have been made into the nature of the cutting forces during ball-end milling [3, 24-32]. By utilization of the previously proposed methods, the motivation in this study is to form a comprehensive and practical model that is validated through various cutting conditions. Since accurate prediction for the cutting forces is aimed a mechanistic approach is employed. Calibration tests are required to be made for each material/tool combination in order to determine the specific cutting constants in the model; however the resulting model is supposed to be making satisfactory predictions for all cutting types in all cutting directions.

Although the utilized calibration method involves certain changes, mainly the method of Altintas [1] for mechanistic identification of cutting constants in milling has been employed. The cutting force model is built upon the previous studies of Lazoglu [3], where a Boolean approach is used for detection of engagement regions, and resulting surface topography can also be determined together

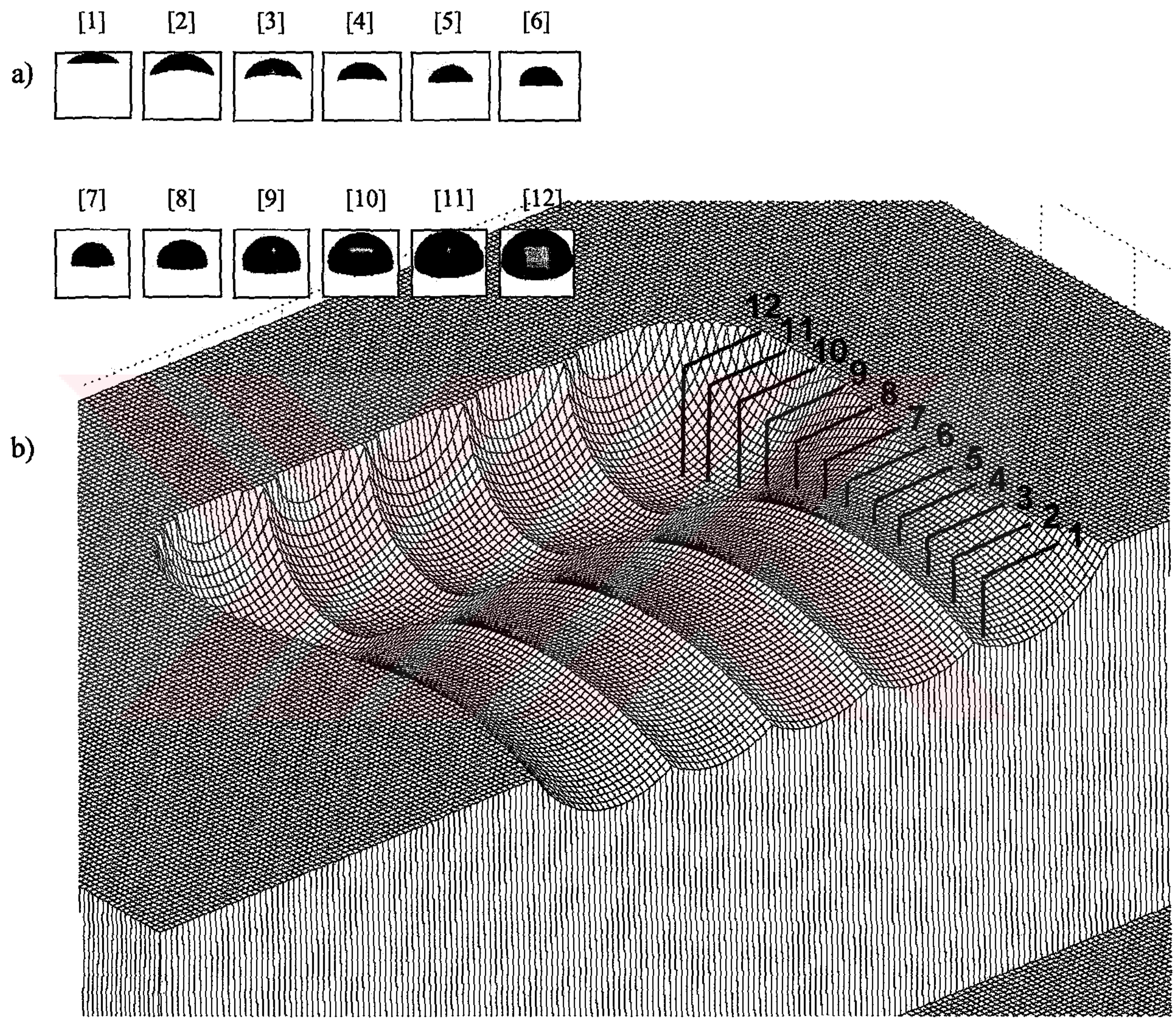

Figure 3.7: a) Projections of engagement domains into x-y plane at various locations
b) Machined workpiece simulation output for a convex cut realized in 5 steps

with the cutting forces for given cutter/workpiece geometry, process parameters and tool path. After explaining the details of the chip load model, the employed force model is described in this chapter.

3.4.2 Chip Load Model

In order to determine the differential cutting forces at any cutter point in the engagement domain, the first step to be taken is to find the infinitesimal chip load for such a discrete element. Thereafter, for the chip load to be evaluated, chip thickness must be known.

As previously mentioned, the chip thickness formulation proposed by Martelotti (Equation 2.1) has been utilized. The geometry and chip formation of a straight-end milling operation is displayed in Figure 3.8. The formulation for straight-end mills has been modified, since the chip thickness varies along the cutting edge as the depth of cut is changed.

The instantaneous undeformed chip thickness for ball-end mill cutter is found as follows,

$$(t_c)_{kn} = t_x \cdot \sin(\theta) \cdot \sin(\psi) \cdot \varepsilon_{kn} \qquad (3.8)$$

where t_x [mm/rev-tooth] is the feed-per-tooth-per-revolution, and it is determined from feedrate [mm/min] / $N_f \omega$ [rpm]. N_f and ω represent the number of flutes and spindle speed, respectively. θ is the cutting element rotation angle, and ψ is the cutting element position angle (Fig. 3.2).

$$\varepsilon_{kn} = \begin{cases} 1 & \text{if the } k^{th} \text{ discrete point on the } n^{th} \text{ cutting edge is in engagement with the workpiece.} \\ 0 & \text{otherwise} \end{cases}$$

Therefore, instantaneous infinitesimal chip load for each discrete element which is in contact with the workpiece can be written as the following,

$$dA_c = (t_c)_{kn} \cdot (dz)_{kn} \qquad (3.9)$$

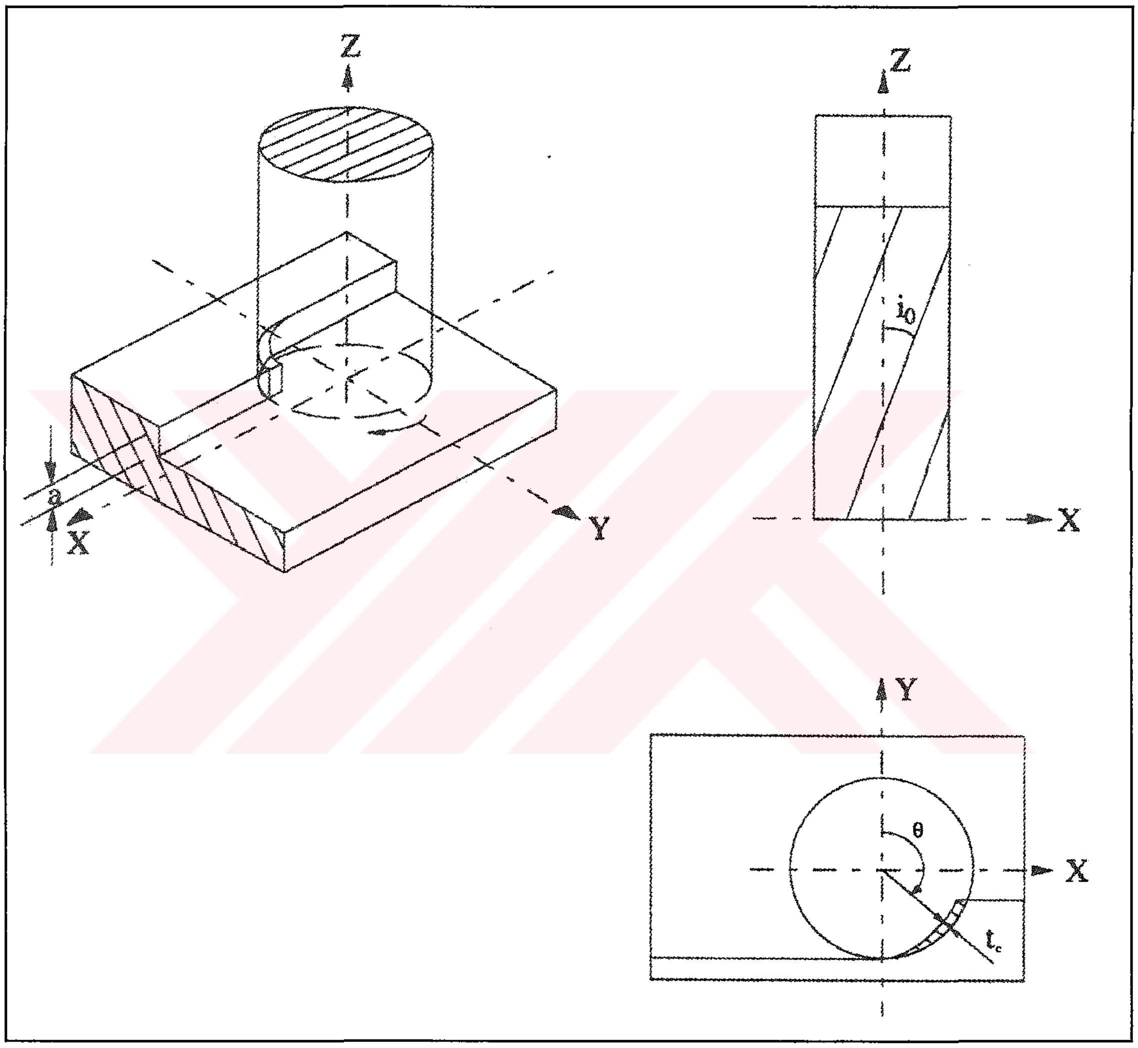

Figure 3.8: Straight-end milling geometry and chip formation

where $(dz)_{kn}$ represents differential chip height along the longitudinal cutter axis at the k^{th} discrete point on the n^{th} cutting edge. See Figure 3.9 for an illustration of the discretized chip load in ball-end milling.

3.4.3 Cutting Force Model

For a differential chip load (dA_c) in engagement domain, the differential radial (dF_r), zenith (dF_ψ) and tangential (dF_t) cutting forces can be written as follows [1],

$$\begin{aligned} dF_r &= K_{rc} \cdot dA_c + K_{re} \cdot dz \\ dF_\psi &= K_{\psi c} \cdot dA_c + K_{\psi e} \cdot dz \\ dF_t &= K_{tc} \cdot dA_c + K_{te} \cdot dz \end{aligned} \tag{3.10}$$

where K_{rc}, $K_{\psi c}$ and K_{tc} are the radial, zenith and tangential cutting constants, and K_{rc}, $K_{\psi c}$ and K_{tc} are the related edge coefficients respectively. These specific cutting energy coefficients vary based on the cutter/workpiece material combination. In order to evaluate these parameters, calibration tests were performed with ball-end mill cutter and an Al7039 workpiece material which also has been used in the model validation tests. The 6 mm radius cutter has been divided into 7 separate disks along the cutter axis in the ball section and cutting constants were evaluated for each region individually by performing incremental slot cutting runs with different feeds at the calibration phase (See Chapter 4 for a detailed description of the calibration process).

Once differential radial, zenith and tangential components, dF_r, dF_ψ and dF_t respectively were obtained through use of Equation 3.10, these cutting force components can be easily transformed into the X-Y-Z global coordinate system as the following,

$$\left. \begin{bmatrix} dF_X \\ dF_Y \\ dF_Z \end{bmatrix} \right|_{k,n} = A \cdot \left. \begin{bmatrix} dF_r \\ dF_\psi \\ dFt \end{bmatrix} \right|_{k,n} \tag{3.11}$$

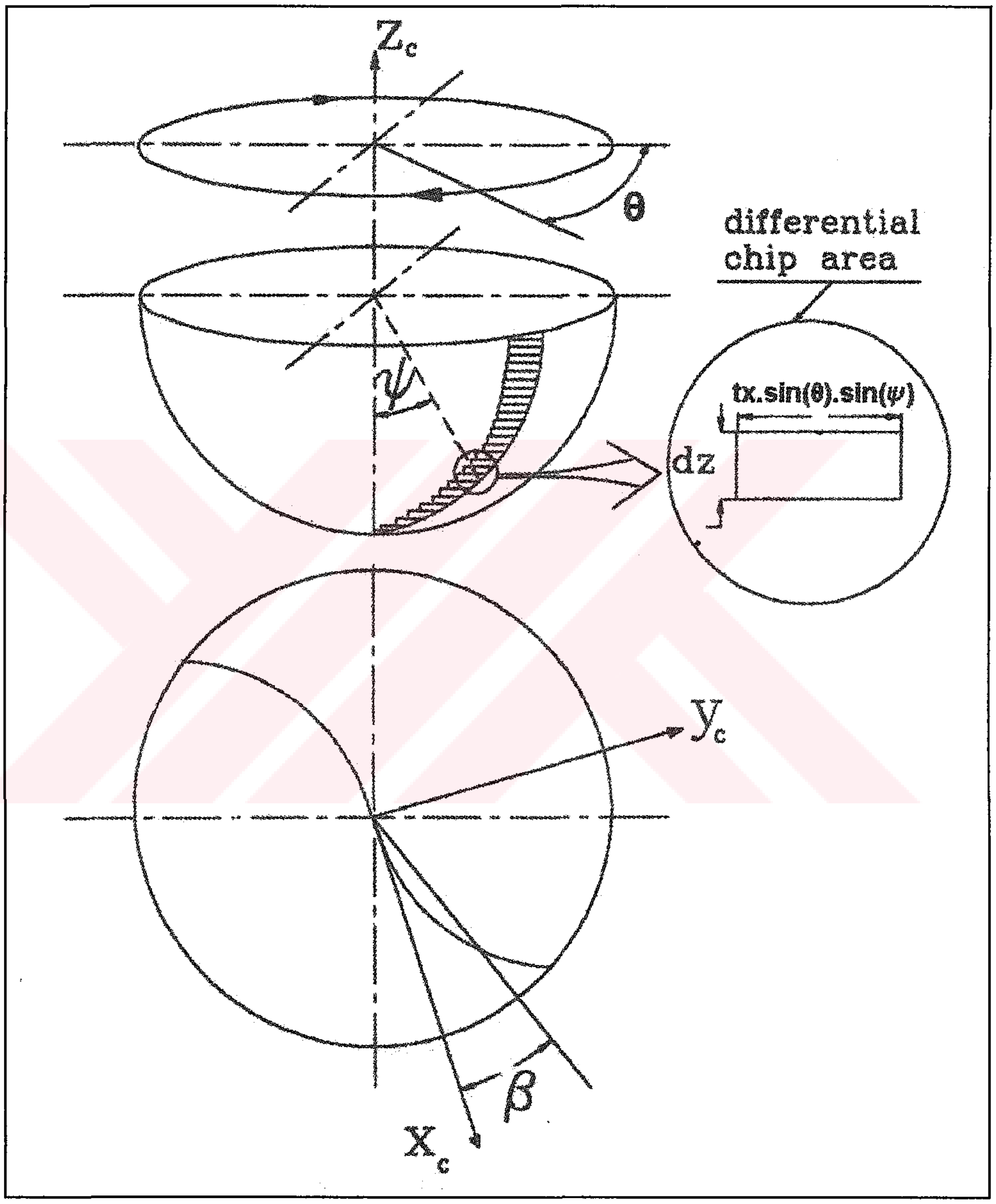

Figure 3.9: Illustration of the discretized chip load in ball-end milling.

$$\begin{bmatrix} F_X \\ F_Y \\ F_Z \end{bmatrix} = \sum_{n=1}^{N_f} \sum_{k=1}^{K} \begin{bmatrix} dF_X \\ dF_Y \\ dF_Z + dF_{pres} \end{bmatrix} \Bigg|_{k,n} \tag{3.12}$$

$$A = \begin{bmatrix} -\sin(\psi)\cdot\sin(\theta) & -\cos(\psi)\cdot\sin(\theta) & -\cos(\theta) \\ \sin(\psi)\cdot\cos(\theta) & \cos(\psi)\cdot\cos(\theta) & -\sin(\theta) \\ \cos(\psi) & -\sin(\psi) & 0 \end{bmatrix} \Bigg|_{k,n} \tag{3.13}$$

$$\theta = \Omega + \frac{(n-1)\cdot 2\pi}{N_f} - \beta_k; \quad n = 1 \ldots N_f \tag{3.14}$$

where K represents the total number of discrete points on a cutting edge, Ω is the cutting edge rotation angle and β is evaluated from Equation 3.5 (see Figure 3.2 for an illustration of the cutting force components and angular relationships). One important aspect of the model to mention here is the additional dF_{pres} force that is included to dF_Z. This force is assumed to result from a constant pressure value existing over the workpiece as long as the cutter moved down into the workpiece in the z direction. Its amplitude equals this constant pressure times the area of the cutter/workpiece contact region. Additional tests have been performed in the calibration phase to detect the constant pressure [MPa] as a function of feedrate(f) [mm/min] (details of this procedure is given in Chapter 4 as well),

$$P(f) = 0.0004 \cdot f^3 - 0.0409 \cdot f^2 + 1.8767 \cdot f + 4.3248 \tag{3.15}$$

Next step after prediction of cutting forces was to validate these predictions by performing various validation tests. Validation tests and their results are explained in Chapter 5. A summary chart of the proposed mechanistic approach is supplied in Figure 3.10.

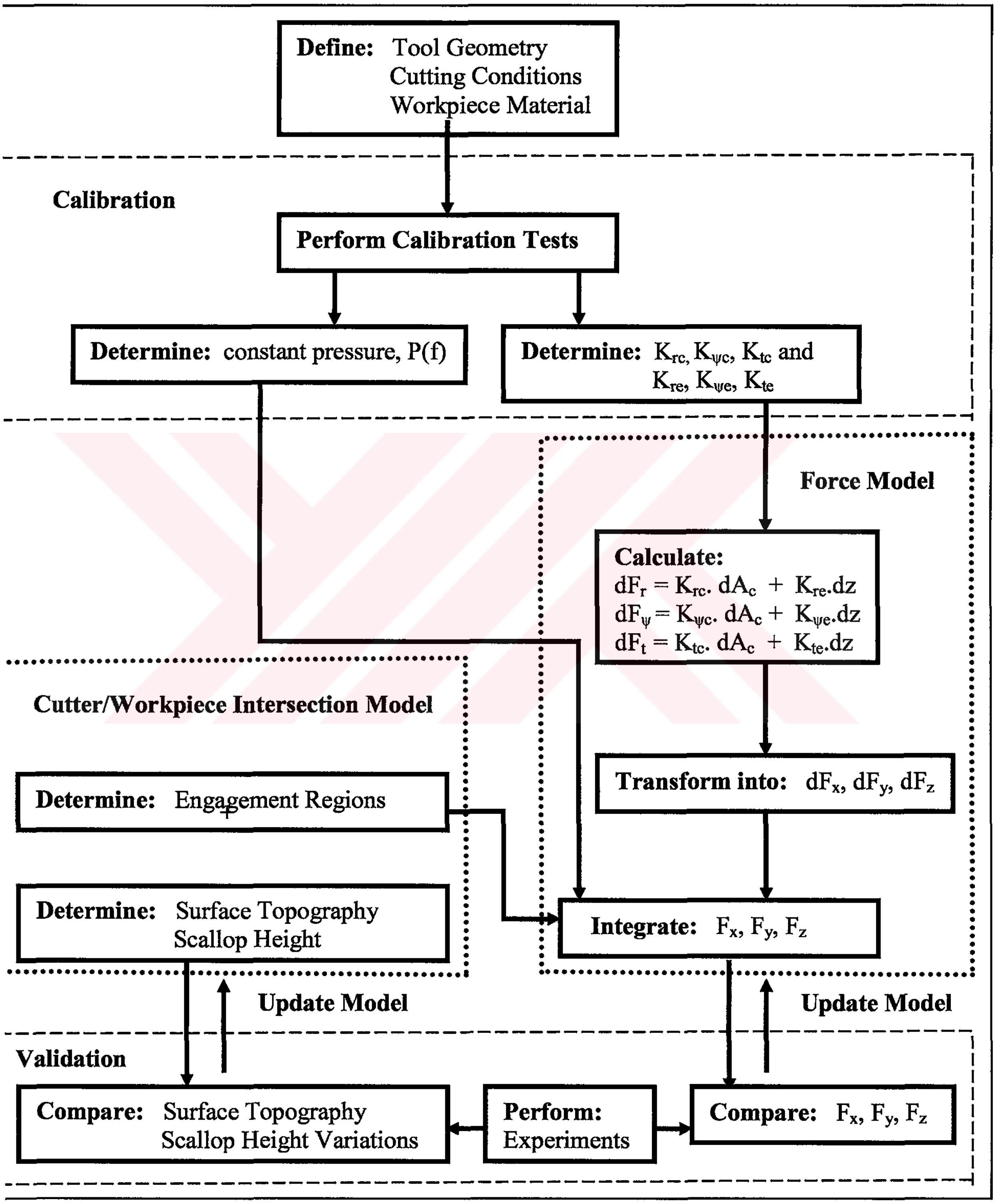

Figure 3.10: A summary chart of the proposed mechanistic approach.

Chapter 4

CALIBRATION PROCESS

4.1 Determining the Cutting Coefficients

Using orthogonal cutting parameters such as shear angle, shear stress, and friction coefficient to determine oblique milling constants is desired for modeling a variety of milling cutter geometries. However, orthogonal calibrations require turning tests and a quick method of calibrating the milling tools will be using a mechanistic approach at that time.

In order to determine the cutting constants in this study, Altintas' [1] approach for identification of cutting constants in milling has been utilized with certain changes.

The experiments for validation were performed on Mazak FJV-200 UHS Vertical Machining Center (VMC). The cutter was carbide ball-end mill cutter from CoroMill Plura series of Sandvik with 12 mm diameter, 37 mm projection length and 30 degrees helix angle (See Chapter 3 for a detailed analysis of the cutter). The workpiece materials were aluminum blocks (Al7039) of size 250x170x38 [mm]. Kistler 3-component dynamometer (Model 9257B) and a charge amplifier have been used to measure cutting forces. The 3-component dynamometer has been fixed to the machine table using fixtures and the aluminum block was attached to the dynamometer using four 8M screws as seen in Figure 4.1.

The cutting forces are sensed by the piezoelectric transducer in the dynamometer and an electric charge output is the outcome of this process. This electric charge is later taken by the charge amplifier and converted into voltage output. The sensitivity values for the three channels (x, y and z) in the amplifier were -7.87, -7.90, and -3.69 pC/N respectively. Amplifier gain for the device was set to 100 for all channels. Subsequently, through use of a proper data acquisition card and software, the voltage output is displayed and recorded as cutting forces in Newton. Displaying and recording of the

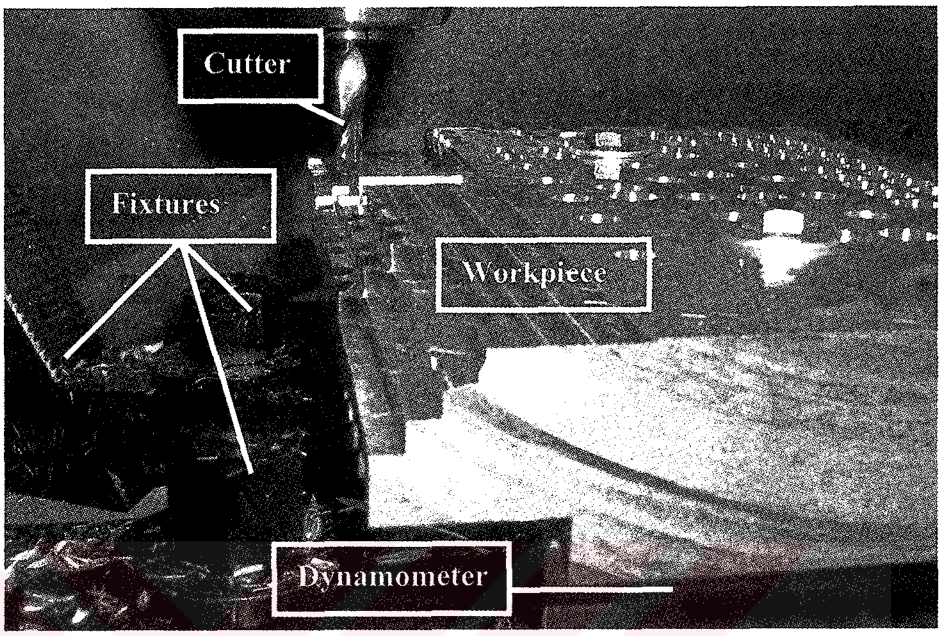

Figure 4.1: Workpiece and 3-component dynamometer fixed to VMC machine table for cutting tests

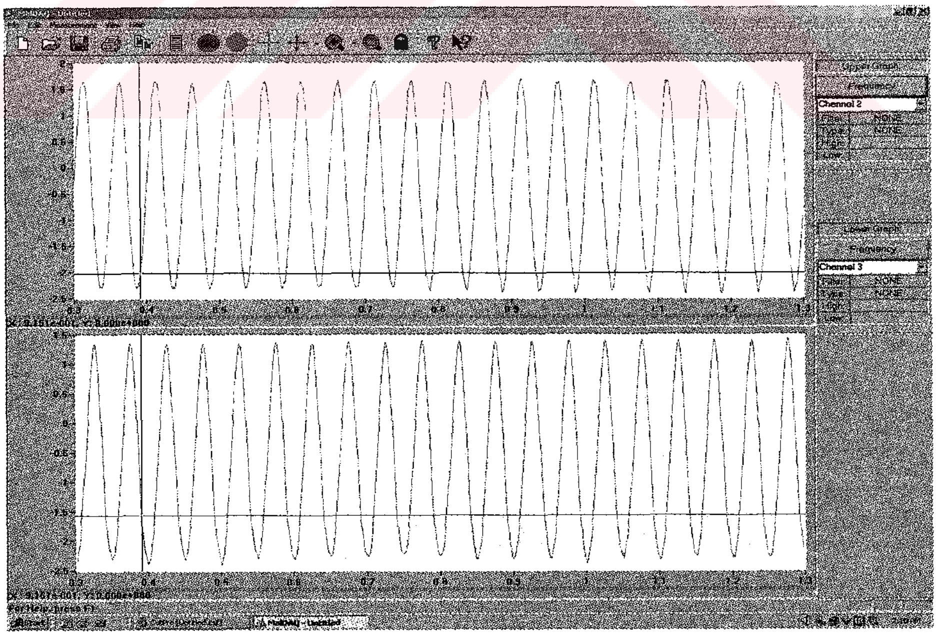

Figure 4.2: Sample output screen in CutPro for cutting forces

measured data was realized with a data acquisition program, MALDAQ module of CutPro (See Figure 4.2 for a sample output screen of CutPro). The complete testing environment can be seen in Figure 4.3.

First step to be taken is to obtain the cutting forces by conducting a set of milling experiments at different feedrates. The 12-48 mm/min feedrate interval has been tested in this study. The ball part of the ball-end mill has been divided into 7 regions for a detailed analysis. Assuming the tip to be at zero level, these intervals were subsequently at 0-0.5, 0.5-1, 1-1.5, 1.5-2, 2-3, 3-4, 4-6 mm distance from tip. Each interval has been tested for four different feedrates; 12, 24, 36 and 48 mm/min. The spindle speed (ω) was kept constant at 600 rpm. Data has been collected for 1 second and with sampling frequency rate (f_s) of 1000 Hz at all tests. Two sets of experimental runs have been performed in order to increase reliability of results. The collection of data is made at every discrete rotation angle $\Delta\theta$ degrees ($\Delta\theta$ is 3.6° for the system under investigation):

$$\Delta\theta = \frac{2\pi \cdot \frac{\omega}{60}}{f_s} \tag{4.1}$$

All the cutting forces of the first set of experiments for two revolutions can be seen in Figures 4.4 and 4.5. In order to obtain the cutting coefficients for a certain interval, the following procedure has been applied step by step:

1. The angular phase differences have been detected for all the collected data and by accounting for these differences all experimental force data have been equally aligned.
2. Using the inverse of the transformation matrix given in Equation 3.13; collected force components (F_X, F_Y, F_Z) have been transformed into radial, zenith and tangential components (F_r, F_ψ, F_t).
3. The peak points (maximum values) of all three components (r-ψ-t) of the cutting force have been found for eight of the revolutions in the collected data (ten revolutions have been captured totally for spindle revolution (ω) of 600 rpm and sampling frequency (f_s) of 1000 Hz, two of these have been omitted in calculations to account for phase differences).

a)

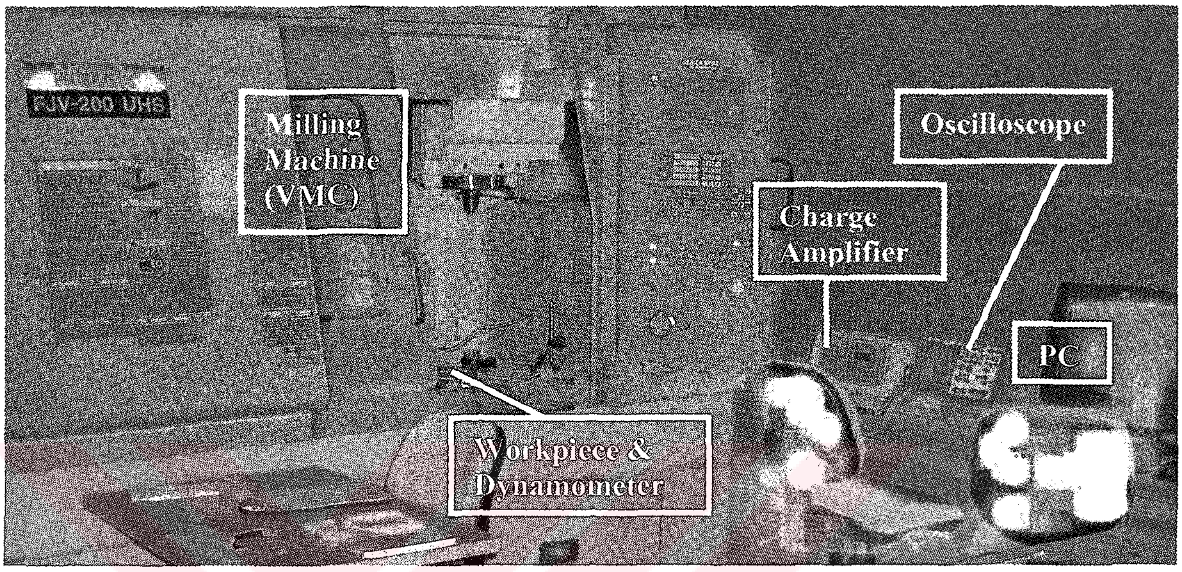

b)

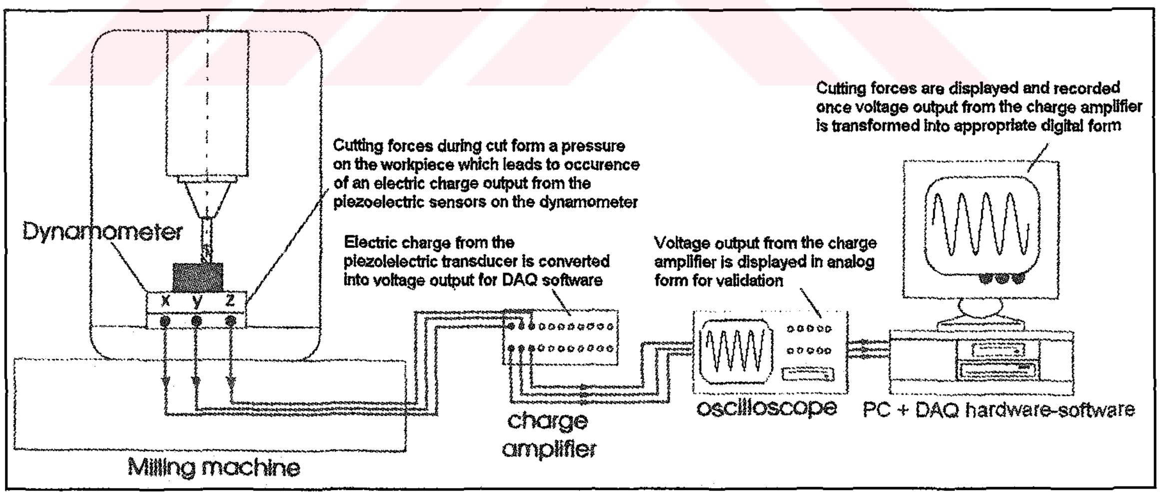

Figure 4.3: The experimental setup for measurement of cutting forces;
a) Actual testing environment, b) Detailed illustration

a)

b)

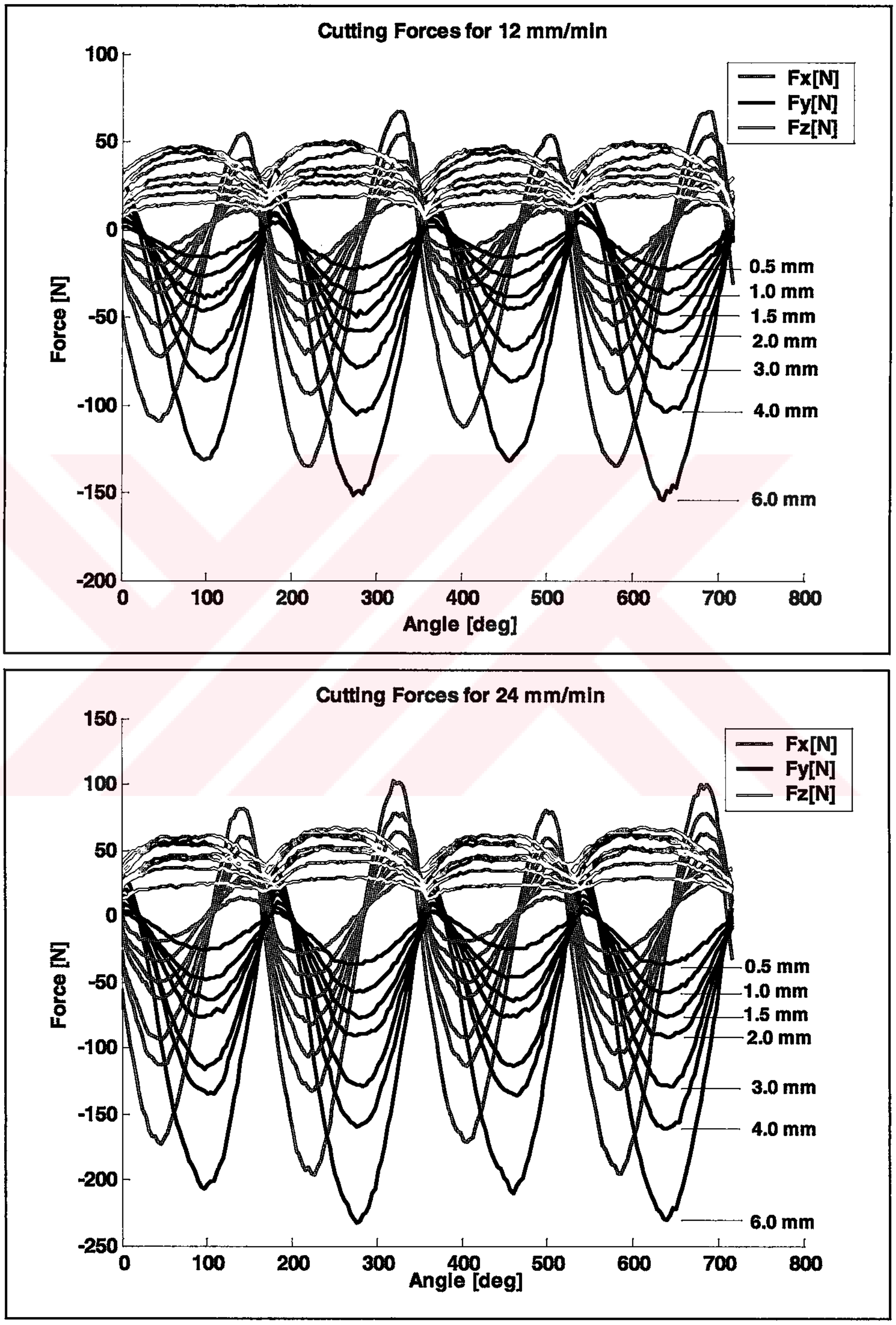

Figure 4.4: Cutting forces corresponding to chosen depth of cuts, at different feedrates; a) 12 mm/min, b) 24 mm/min

a)

b)

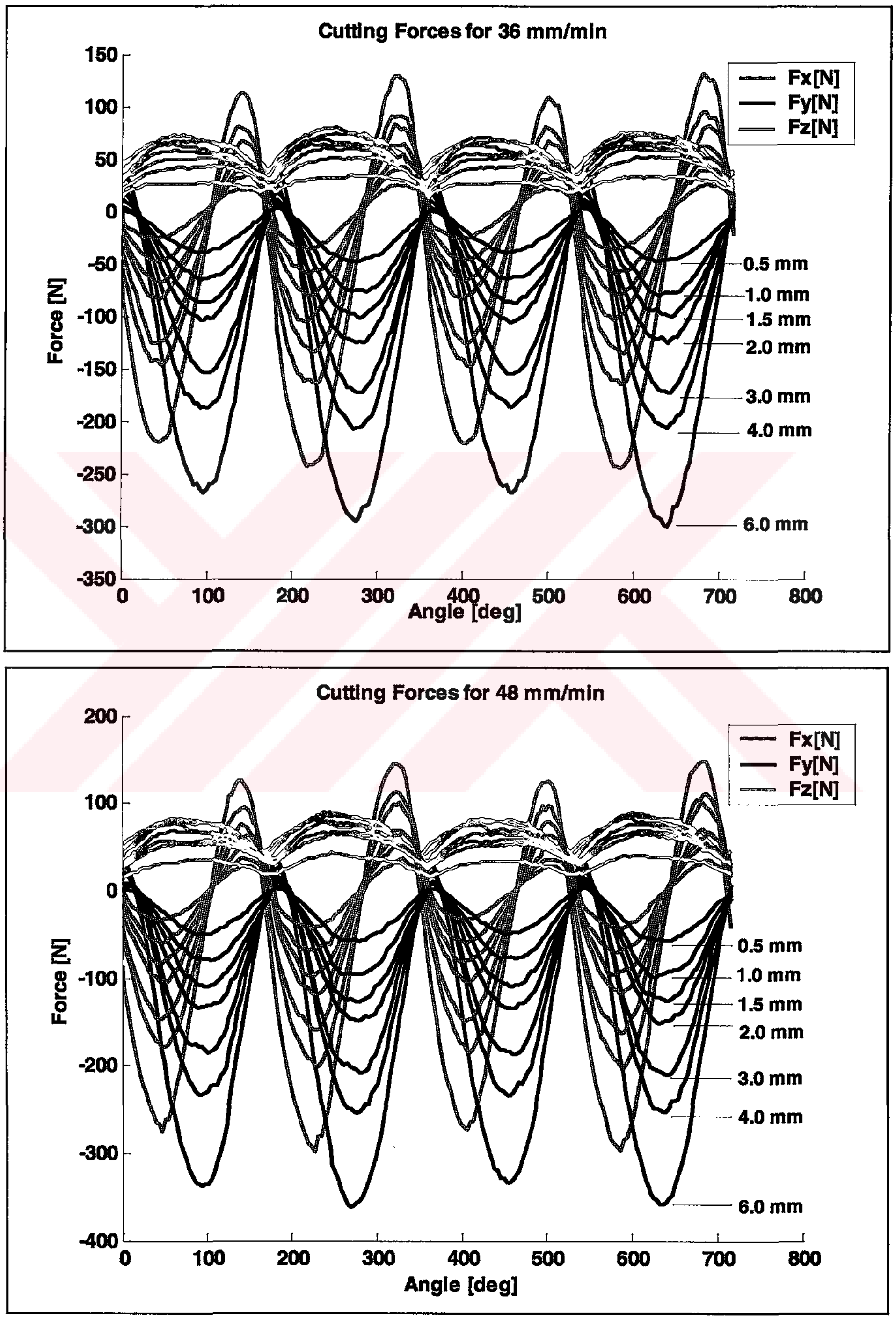

Figure 4.5: Cutting forces corresponding to chosen depth of cuts, at different feedrates; a) 36 mm/min, b) 48 mm/min

4. The differences between the peak points have been obtained and averaged for each increment in the depth of cut (e.g., for the 3-4 mm interval, the cutting forces will equal the difference between 4 mm depth of cut and 3 mm depth of cut tests).

5. Once the F_r, F_ψ, F_t values have been obtained for each depth of cut interval, these have been plotted versus chip thickness in order to obtain the cutting coefficients (Figure 4.6 to 4.9). The determination of cutting constants from experimental data is summarized in Figure 4.10.

The change in cutting coefficients along the cutting edge is displayed in Figure 4.11. It is observed in these plots that other than the $K_{\psi c}$, cutting coefficients sharply fall until 2.0 mm distance from the tip. After this level they stabilize at a certain value. K_{tc} is the most dominant cutting coefficient. The edge coefficients, on the other hand, exhibit an almost completely random behaviour; no trend can be clearly identified by observing their plot.

The numerical values of the cutting coefficients determined with the calibration process can be summarized in the following table:

Table 4.1: Numerical values of cutting and edge coefficients for different intervals from tip.

interval from tip / coefficient	**0 - 0.5 [mm]**	**0.5 -1 [mm]**	**1 - 1.5 [mm]**	**1.5 -2 [mm]**	**2 – 3 [mm]**	**3–4 [mm]**	**4 – 6 [mm]**
K_{rc} [N/mm^2]	**6156**	**2191**	**741**	**398**	**212**	**173**	**16**
K_{re} [N/mm]	**24**	**0**	**7**	**6**	**12**	**3**	**8**
$K_{\psi c}$ [N/mm^2]	**110**	**255**	**433**	**190**	**143**	**123**	**168**
$K_{\psi e}$ [N/mm]	**14**	**19**	**8**	**13**	**6**	**3**	**0**
K_{tc} [N/mm^2]	**10478**	**3327**	**2376**	**1805**	**1404**	**1364**	**1032**
K_{te} [N/mm]	**8**	**9**	**9**	**7**	**11**	**4**	**14**

a)

b)

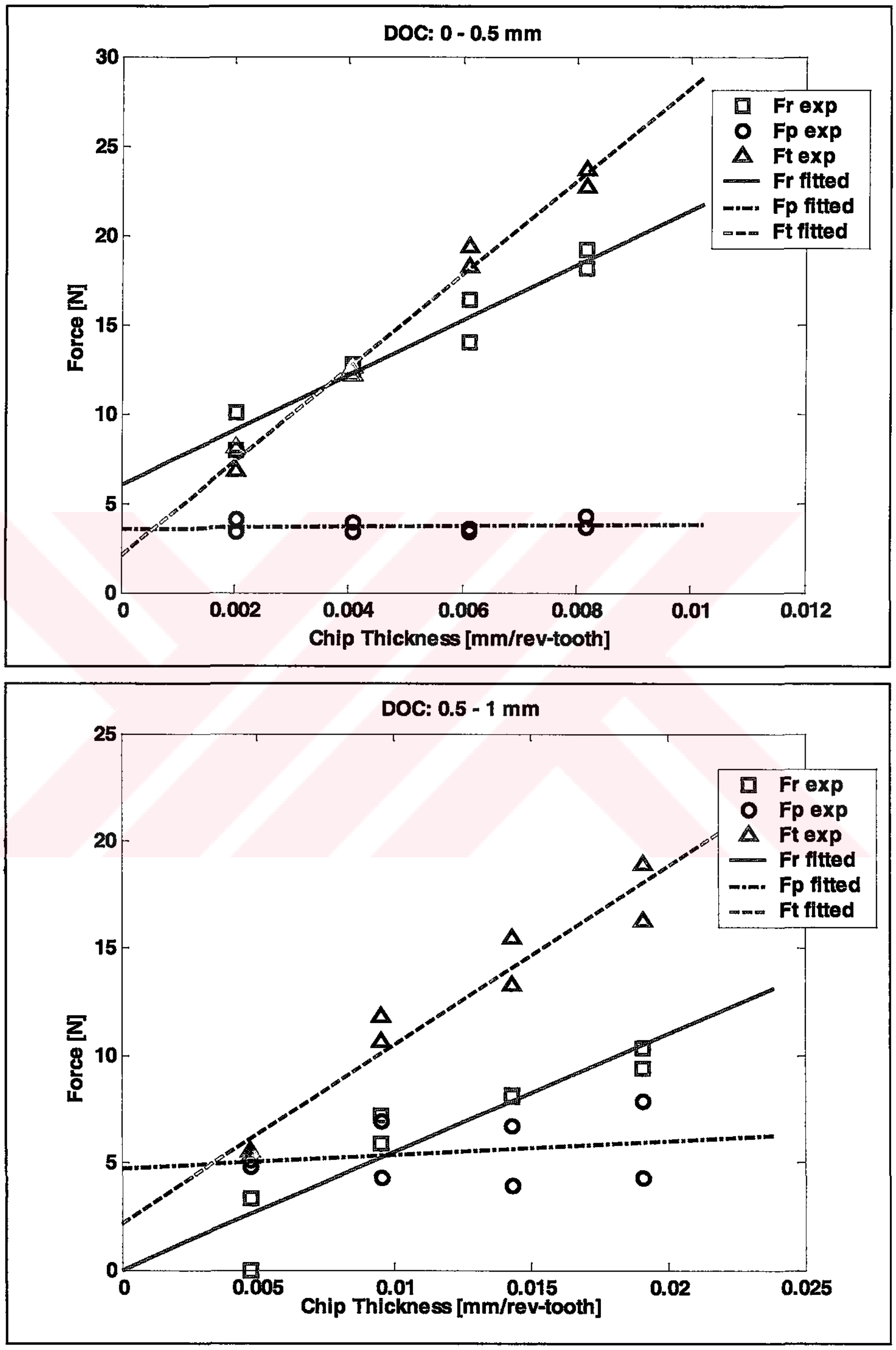

Figure 4.6: Cutting forces vs. chip thickness for different regions of the cutting edge; a) 0 – 0.5 mm, b) 0.5 – 1 mm

a)

b)

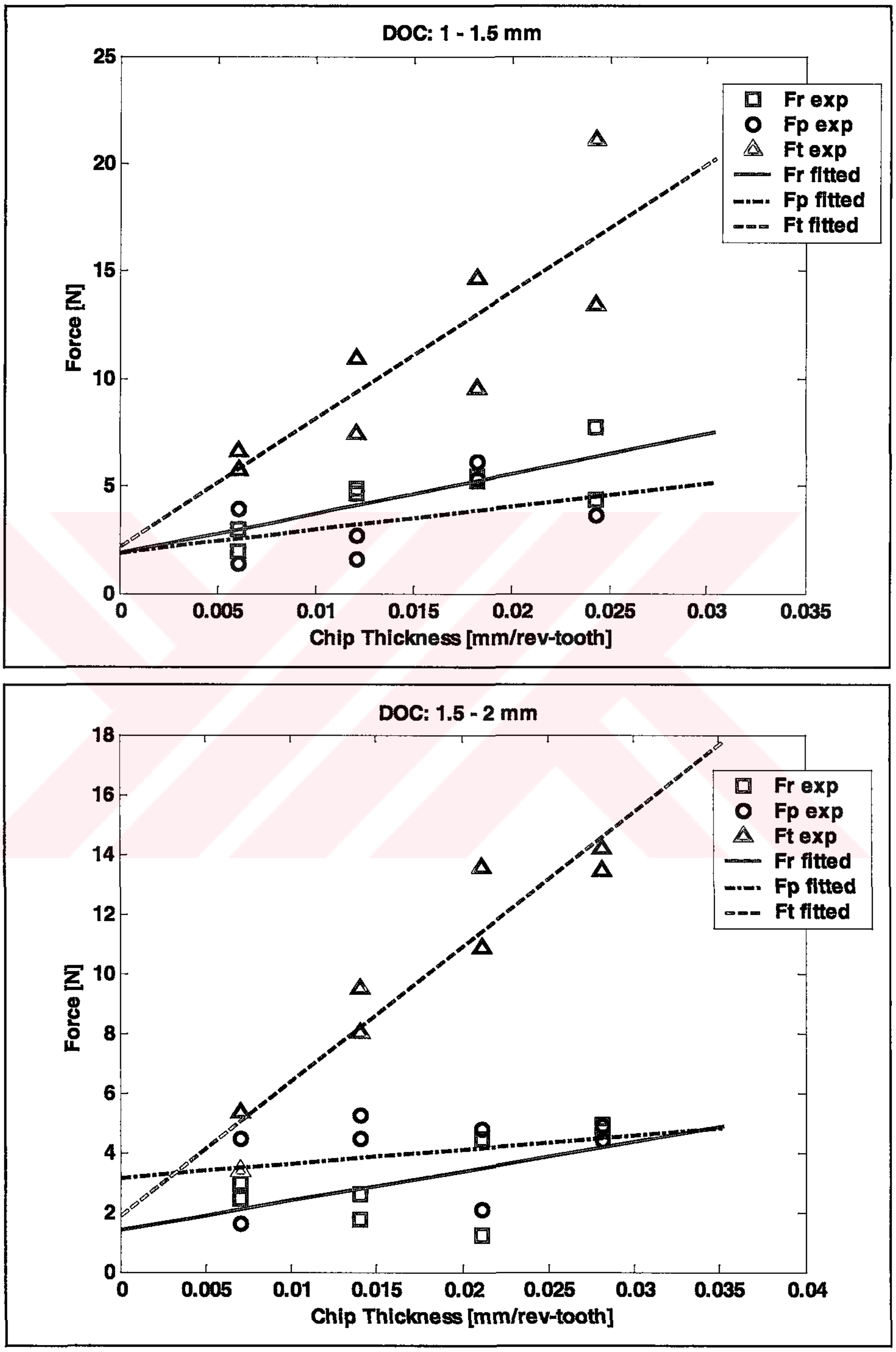

Figure 4.7: Cutting forces vs. chip thickness for different regions of the cutting edge; a) 1 – 1.5 mm, b) 1.5 – 2 mm

a)

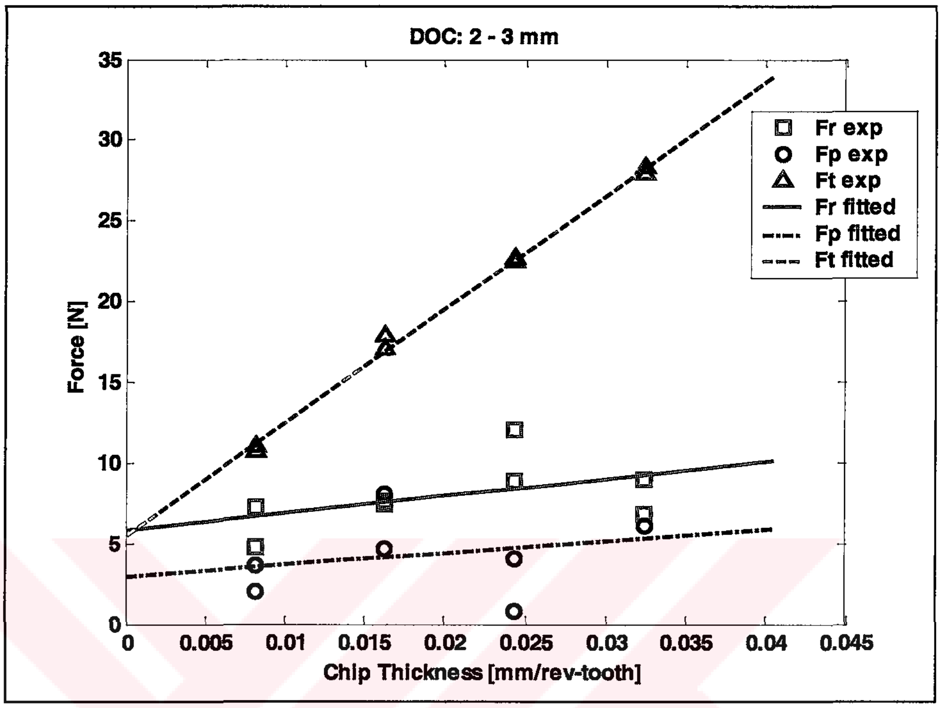

b)

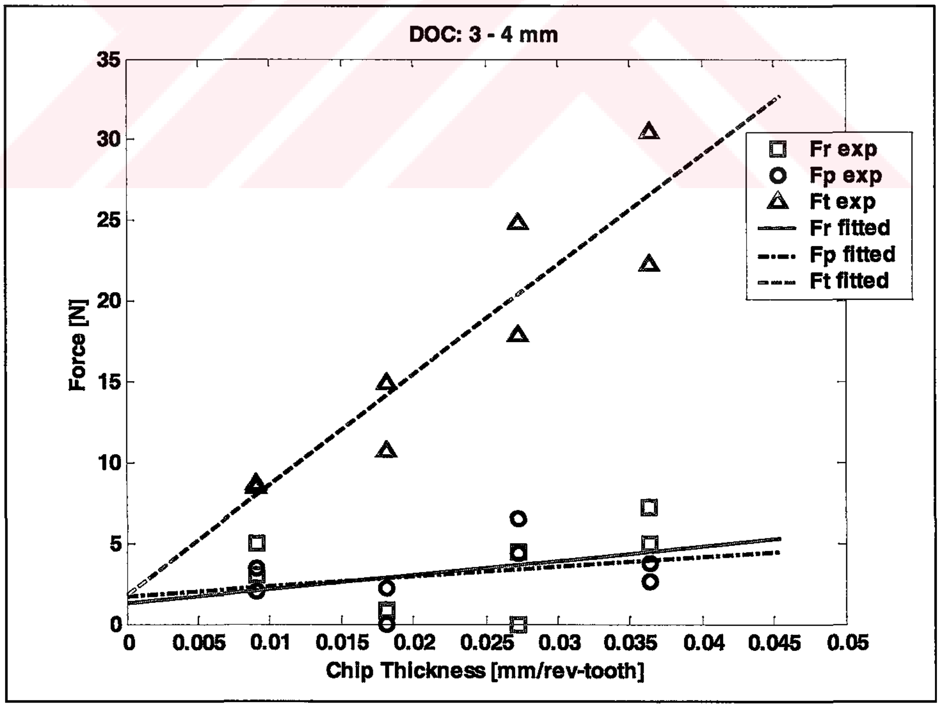

Figure 4.8: Cutting forces vs. chip thickness for different regions of the cutting edge; a) 2 – 3 mm, b) 3 – 4 mm

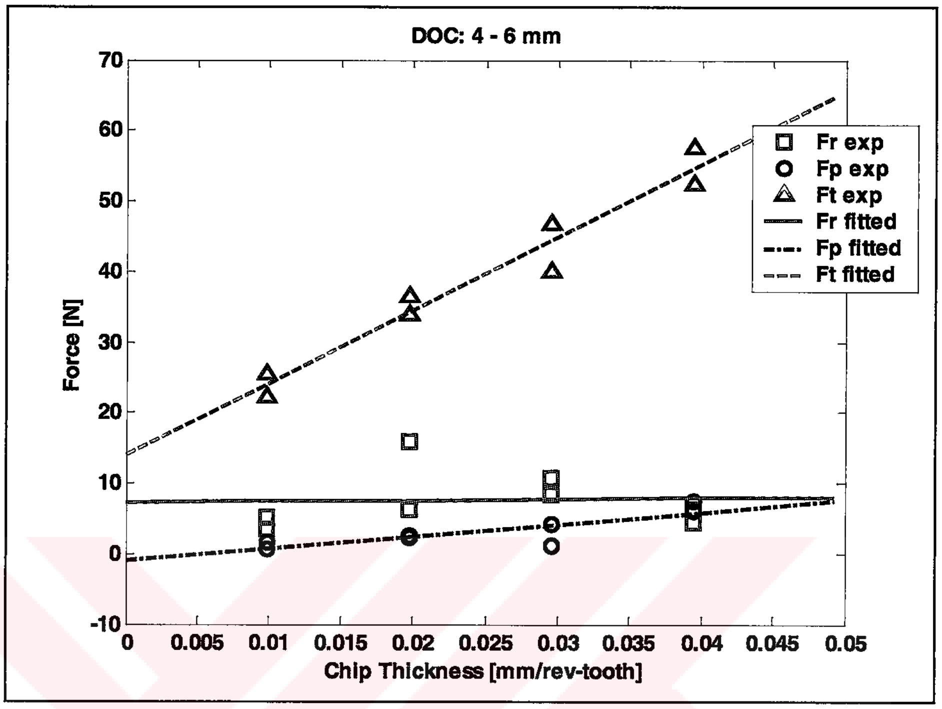

Figure 4.9: Cutting forces vs. chip thickness for different regions of the cutting edge, 4 – 6 mm

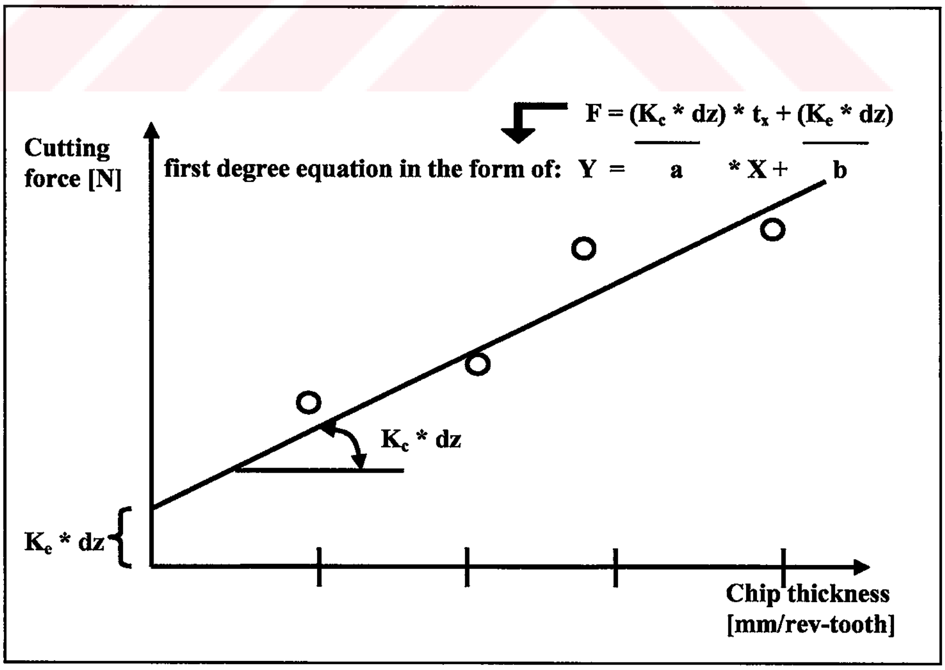

Figure 4.10: Determination of the cutting coefficients from experimental data

a)

b)

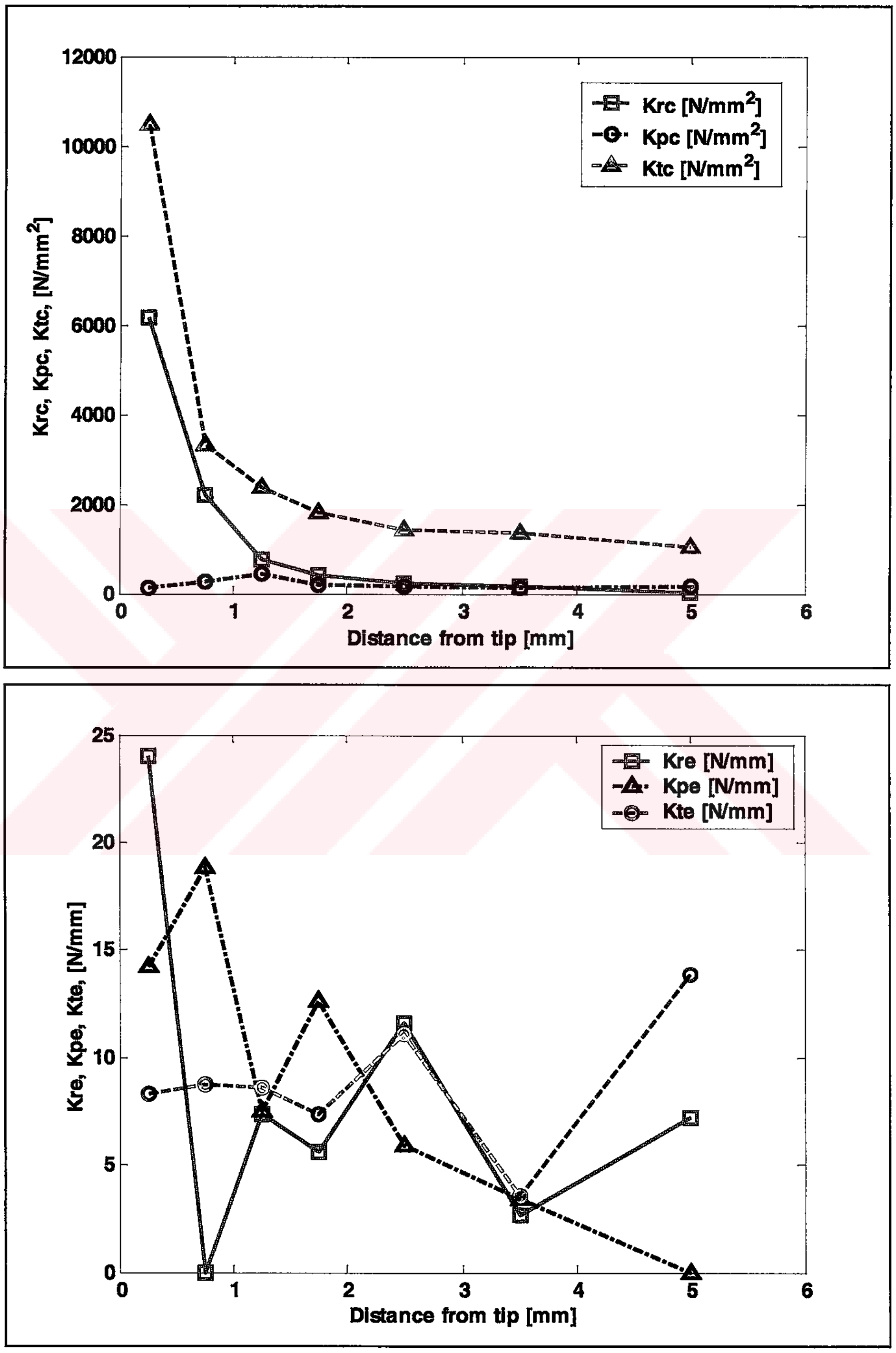

Figure 4.11: The change of coefficients along the cutting edge;
a) cutting coefficients, b) edge coefficients

4.2 Determining the Constant Pressure

Initial validation tests indicated that the force model under-predicted the force in vertical direction, when the cutter has a vertical feed-motion component 'into' the workpiece. This led to the assumption that the spindle was applying a constant pressure on the workpiece surface through the cutter which is proportional to the vertical feed rate into the workpiece. Thorough investigations proved that this assumption, indeed, was true.

The experimental setup in calibration tests has been used for these investigation runs. Vertical feed has been given the values; 0.5, 1.5, 3, 6, 12, 18, 24, 30, 36, 42, 48, 54, 60 mm/min. In order to determine the exerted constant pressure on the workpiece surface, the pressure formula:

$$P = F_z / A \tag{4.2}$$

has been used where F_z is the force in vertical direction and A is the contacting area of the cutter at an instant. The area contacting with the workpiece changes, as the cutter penetrates into the workpiece. This area is calculated numerically using a Matlab code for a certain feedrate. Since the penetration time is discretized for analysis, each incremental increase in the contacting area for a time interval is found and added in order to find the total contacting area at an instant.

The change of the contacting region with respect to time is given in Figure 4.12.a for the vertical feed 36 mm/min and in Figure 4.13.a for the vertical feed 12 mm/min. The cutting force F_z, changing with time is given in Figure 4.12.b and Figure 4.13.b together with the resulting constant pressure for the same feed rate.

The constant pressure values have been found for all tested feed rates and plotted in order to obtain a third degree fitted polynomial for pressure as a function of feed rate (Equation 3.15). Pressure values approached zero as the vertical feed component approached zero. After 10 mm/min vertical feed, the pressure values had a linear trend. The calculated values for the constant pressure can be seen in Figure 4.14 together with the fitted function for constant pressure.

a)

b)

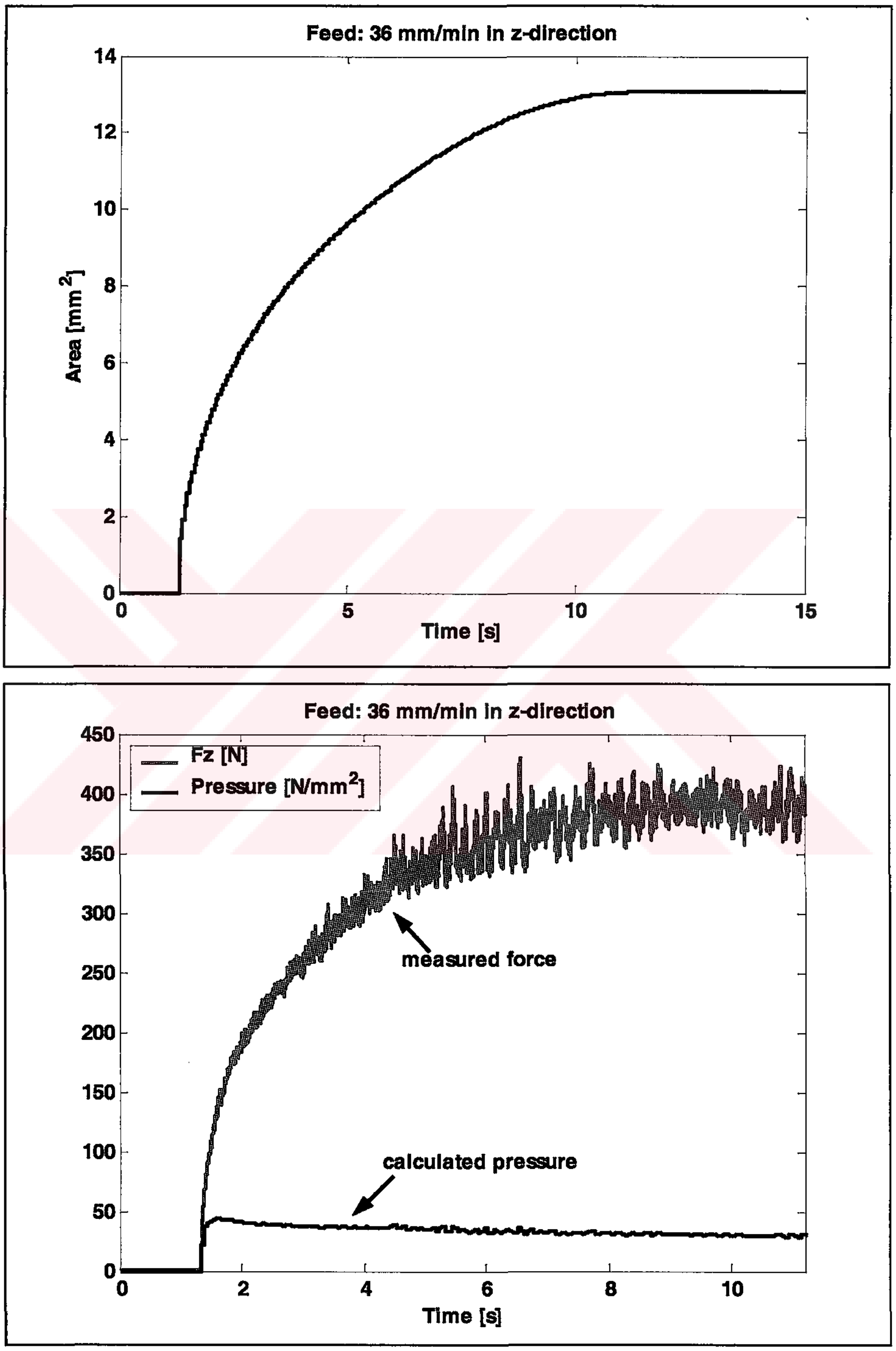

Figure 4.12: a) The change of contact area through vertical cut with feed 36 mm/min
b) The change of cutting forces with feed 36 mm/min and the observed constant pressure

a)

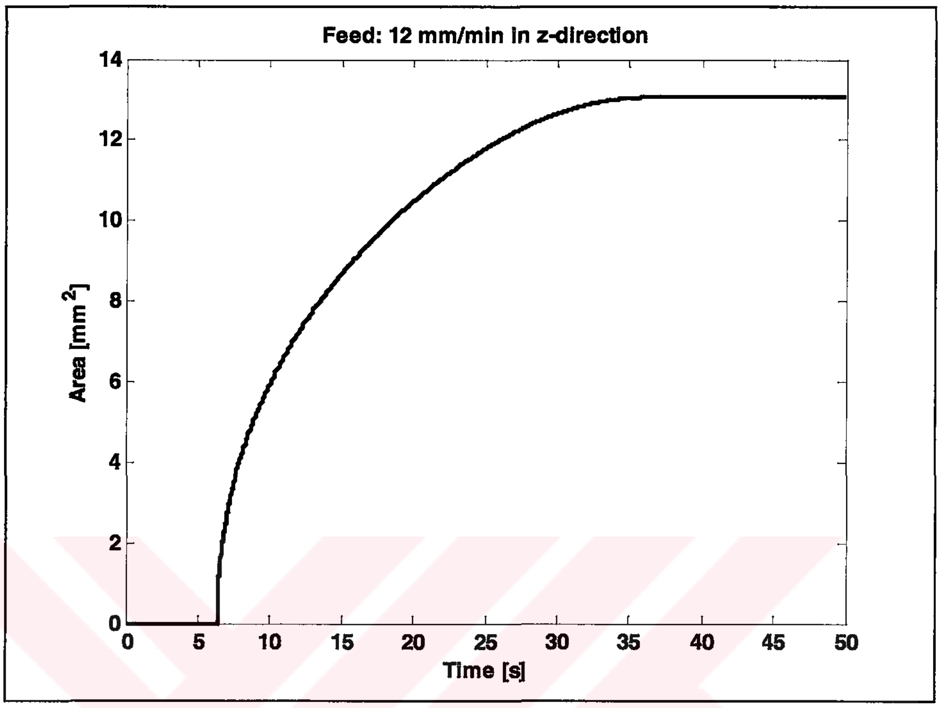

b)

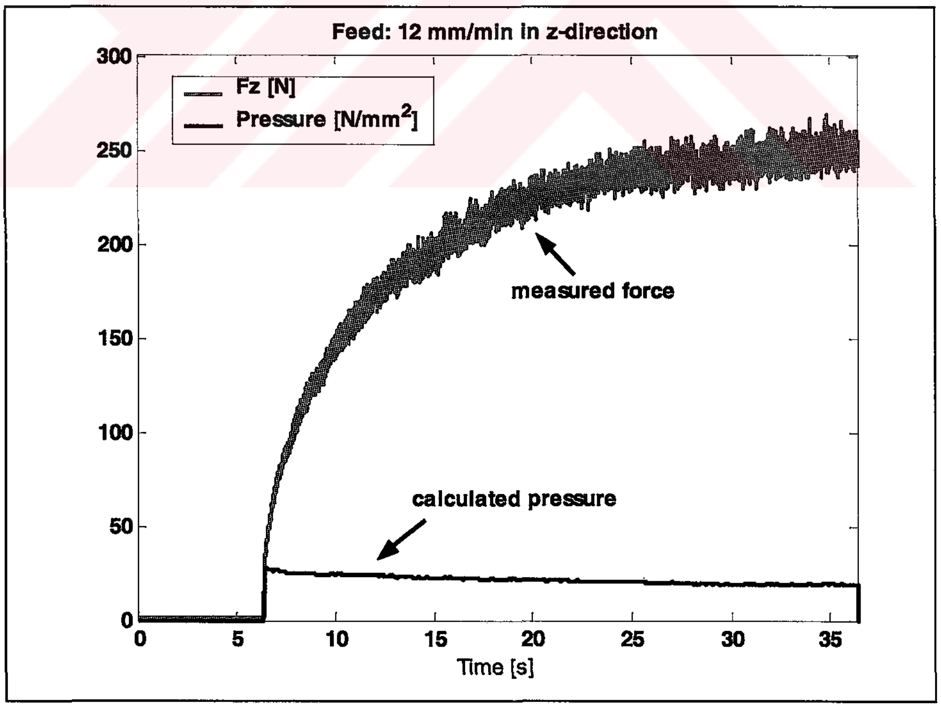

Figure 4.13: a) The change of contact area through vertical cut with feed 12 mm/min
b) The change of cutting forces with feed 12 mm/min and the observed constant pressure

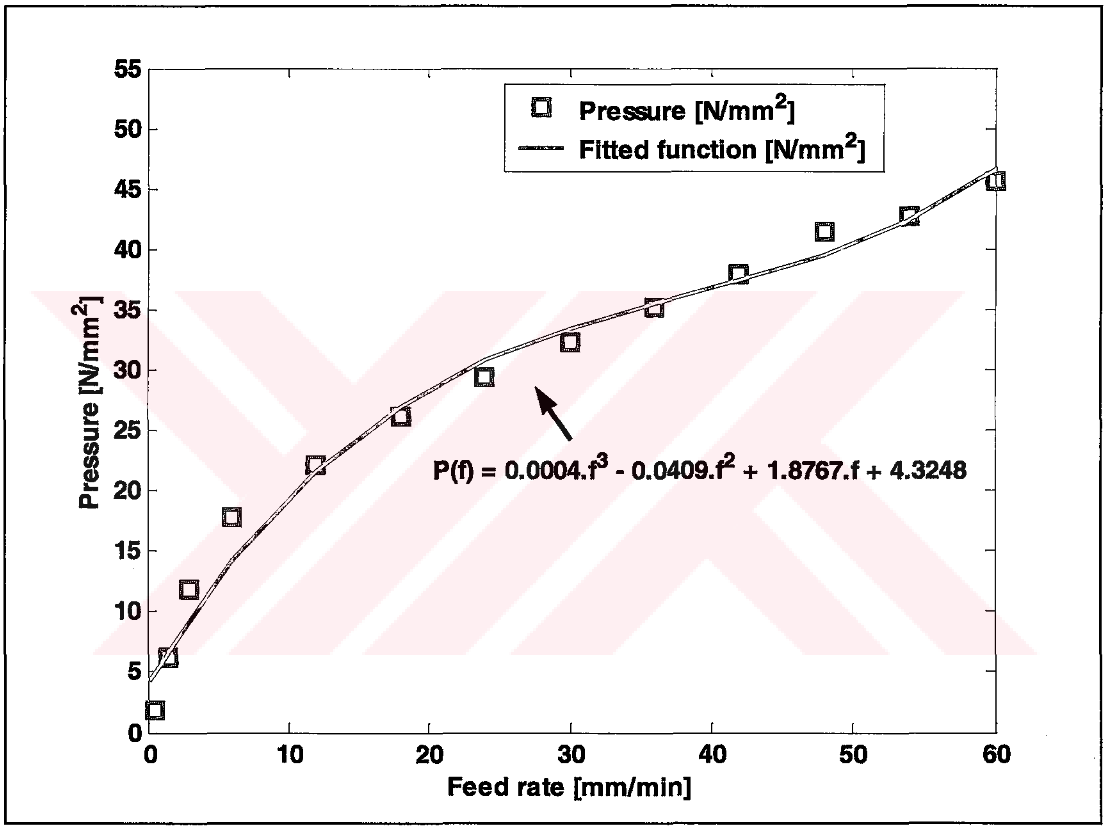

Figure 4.14: The change of cutting and edge coefficients along the cutting edge

Chapter 5

VALIDATION TESTS

5.1 Introduction

Various tests have been performed for validation of the proposed force model. 2½ axis cases have been tested initially and more complicated 'free form' cases have been investigated once satisfactory results have been obtained in 2½ axis milling.

The same experimental setup in calibration has been used in validation tests. The feed rate of the cutter has been chosen to be 48 mm/min in the tests. Cutting has been realized only by ball part of the cutter in all cases. The mesh size in simulations was selected to be 0.1 mm which adequately resembled the actual cutting conditions for the mathematical force model.

The applied conditions and results of the performed cutting tests are described in this chapter. The predicted workpiece topography is given in all cases together with the predicted and measured cutting forces. A sample comparison of predicted and actual machined surface is also provided at the end of the chapter.

5.2 2½ Axis Cutting Tests

5.2.1 Full immersion slot cut

The calibration experiments were performed in the form of slot cuts. As the simplest type of cut in milling, first tests for validation of cutting forces were also slot milling tests.

Slots of various depths have been cut in order to test the model. Cutting has been realized by the ball part of the cutter only. A straight path in x direction has been cut into the workpiece and cutting forces were recorded for 1 s after full immersion occurred in the slot. Cutting conditions are summarized in Table 5.1. The simulation outputs for machined parts are given in Figure 5.1 and Figure 5.2 together with the engagement region after full immersion.

Table 5.1 Cutting conditions for full immersion slot cuts

Test no.	1 – 2 – 3 – 4 – 5 – 6 – 7 – 8
Feed rate	48 mm/min
Depth of cuts	0.5 – 1 – 1.5 – 2 – 3 – 4 – 5 – 6 mm
Spindle Speed	600 rpm
Amplifier gain	100
Sampling frequency	1000
Sampling time	1 s
Tool path	20 mm straight, horizontal in x direction

The prediction of cutting forces in all X-Y-Z directions showed very good agreement with actual force values at higher depth of cuts. Predicted and measured forces are plotted versus rotation angle in Figure 5.3 to Figure 5.6 for various depth of cuts. As the depth of cut level decreased, inaccuracy in the predictions increased due to the increasing influence of runout. The cutter has two flutes, as a result two peaks are observed in a single rotation of the cutter that corresponds to 360 degrees. Resulting forces in two rotations of the cutter is given in the plot. Since different cutting constants are considered for different cutting regions, and the depth of cuts for this test are generally chosen to be on cutting region boundaries, there are steep deviations occasionally especially for smaller depth of cuts.

a)

b)

c)

d)

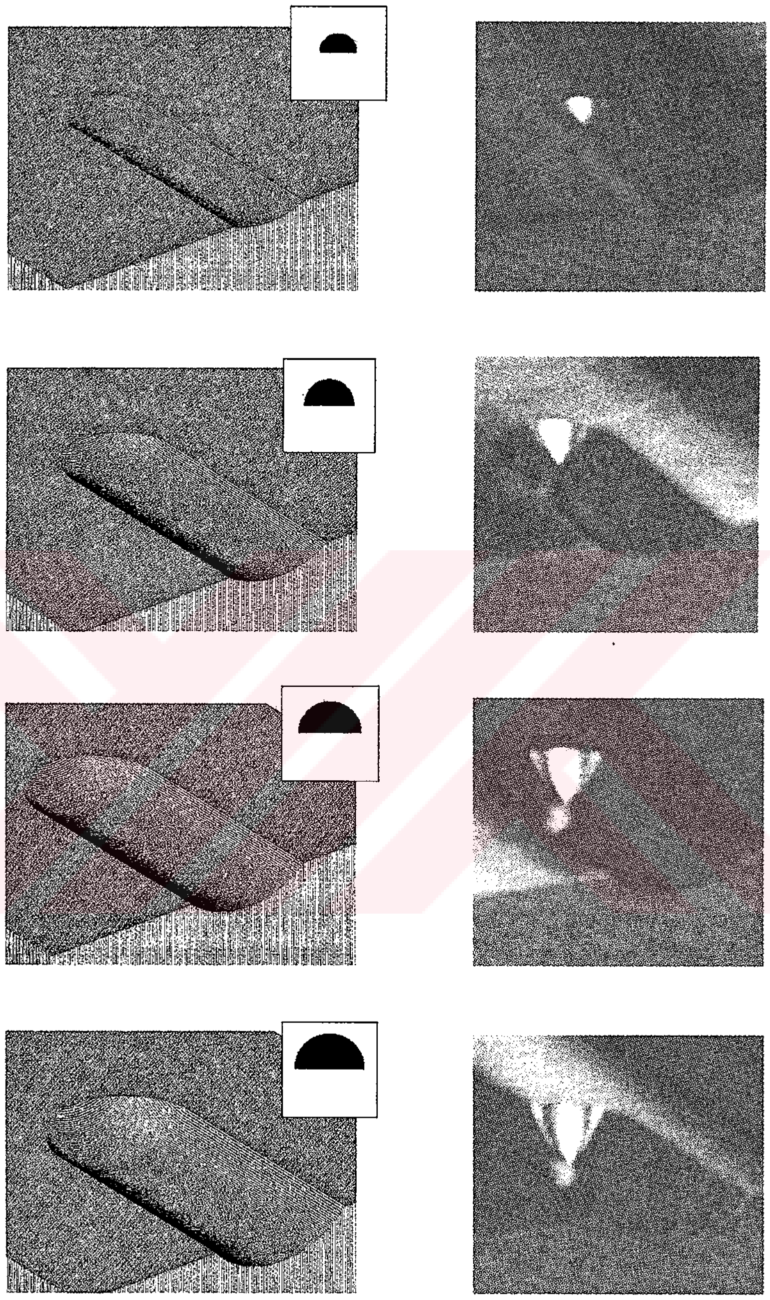

Figure 5.1: Simulation output and related engagement region vs. actual cut for slots of various depth of cut; a) 0.5 mm, b) 1 mm, c) 1.5 mm, d) 2 mm

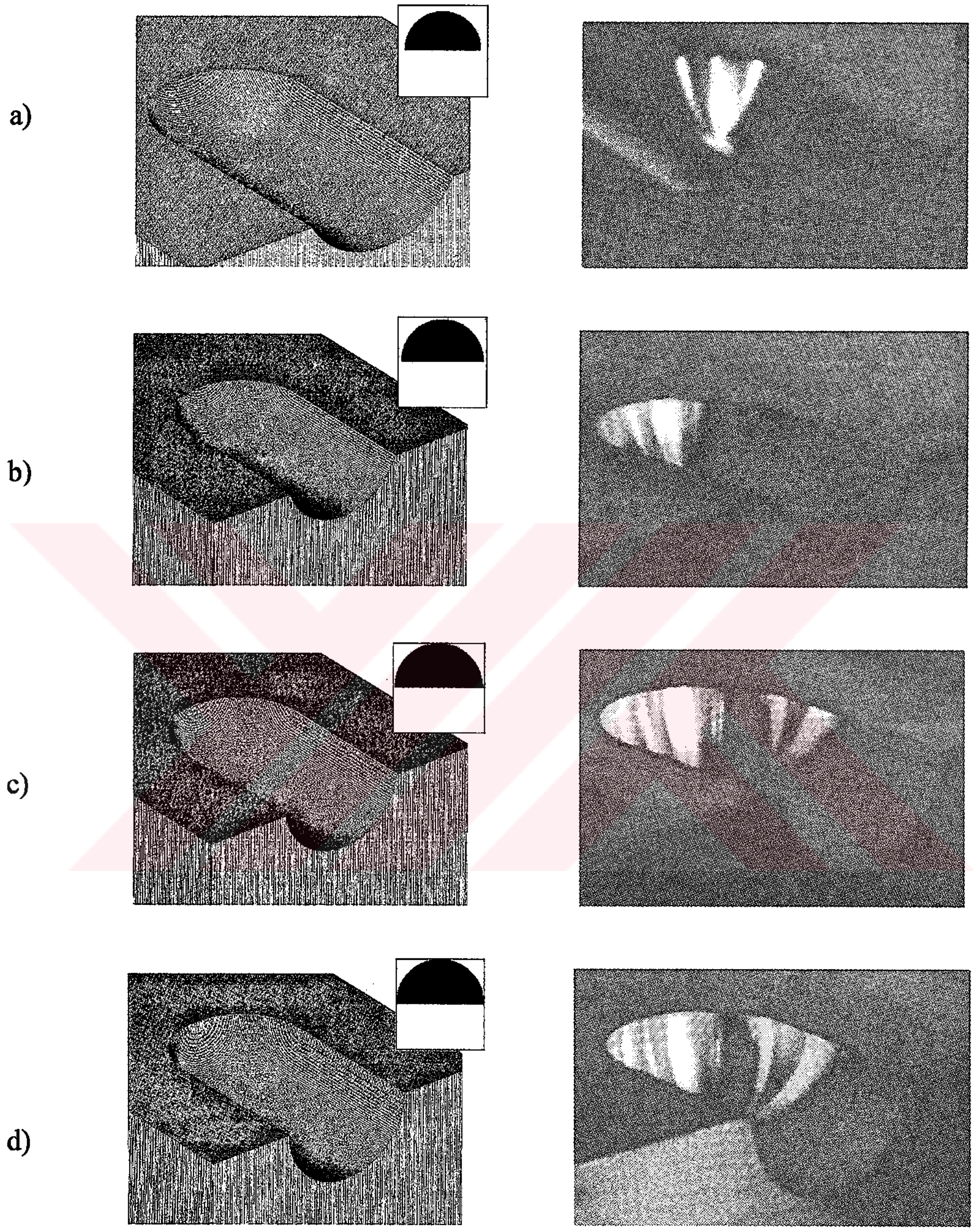

Figure 5.2: Simulation output and related engagement region vs. actual cut for slots of various depth of cut; a) 3 mm, b) 4 mm, c) 5 mm, d) 6 mm

a)

b)

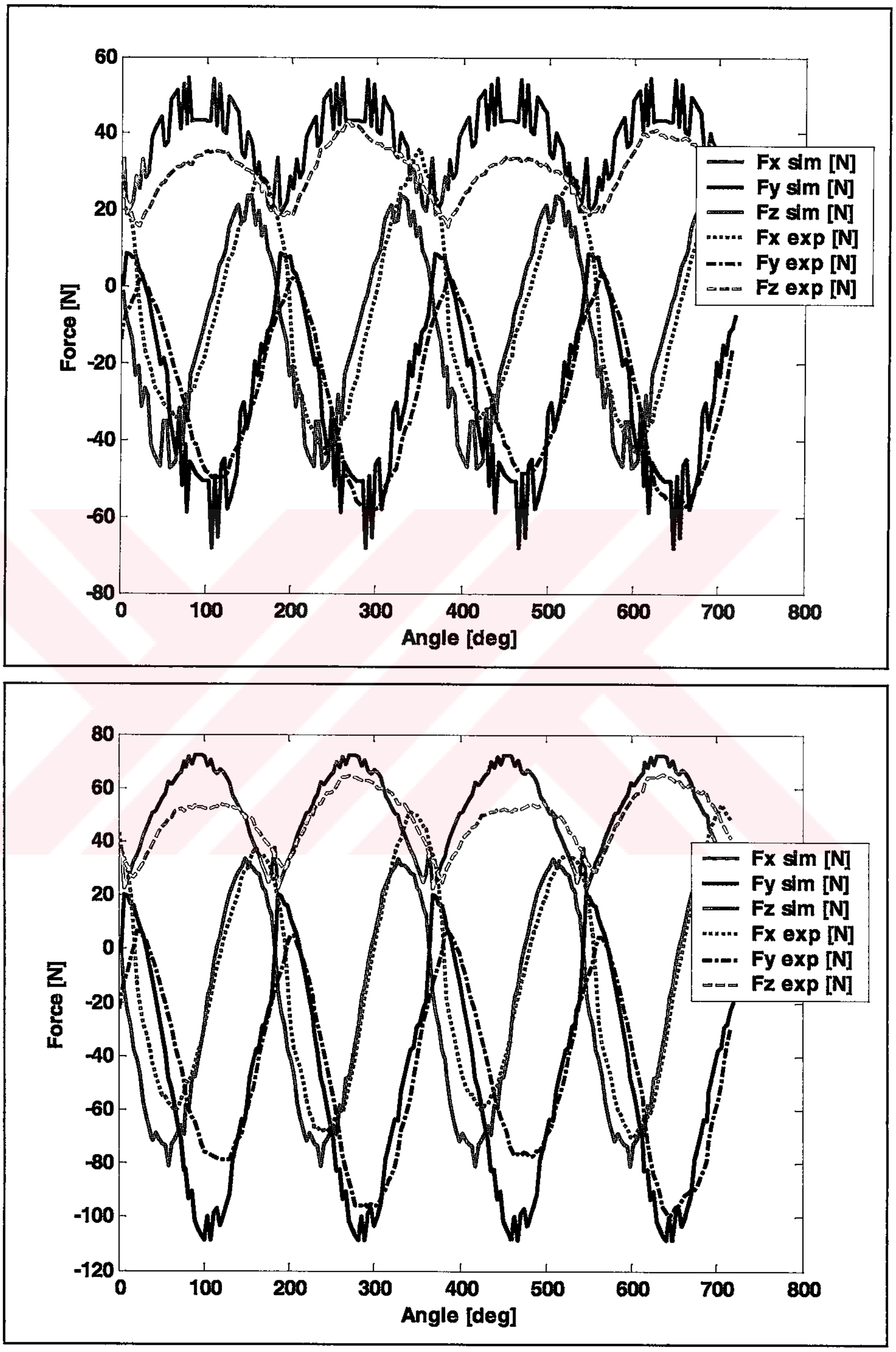

Figure 5.3: Predicted and measured forces vs. angular advance for;
a) 0.5 mm depth of cut b) 1 mm depth of cut

a)

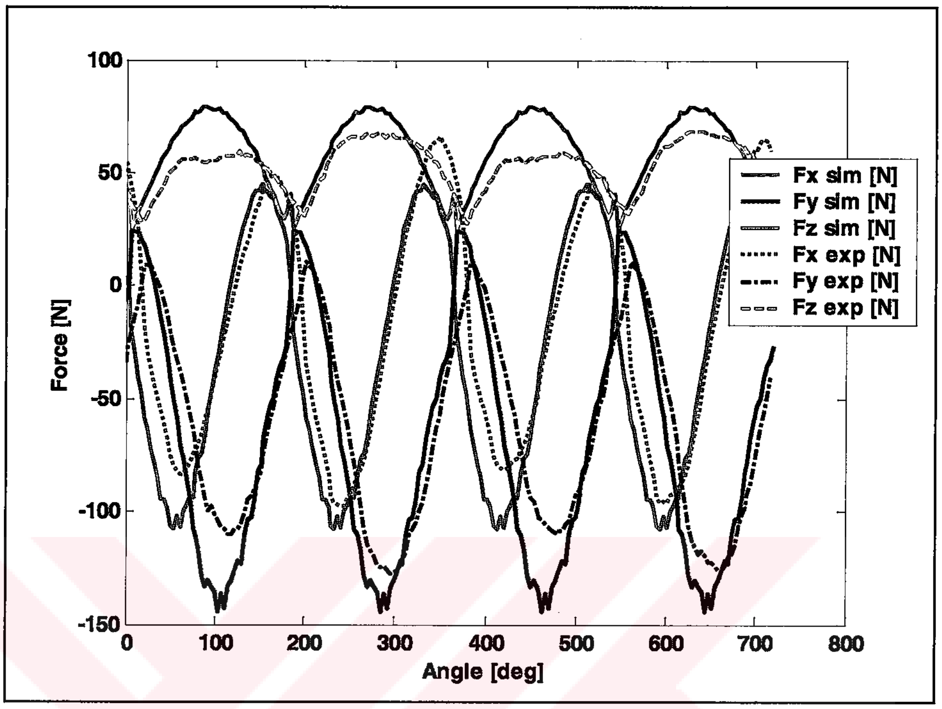

b)

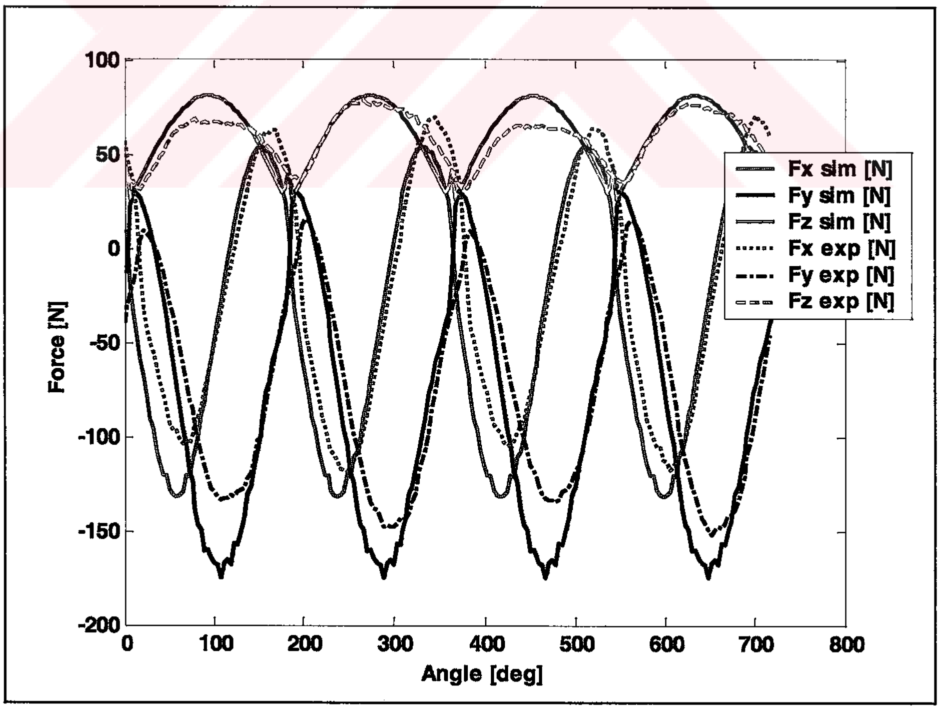

Figure 5.4: Predicted and measured forces vs. angular advance for;
a) 1.5 mm depth of cut b) 2 mm depth of cut

a) 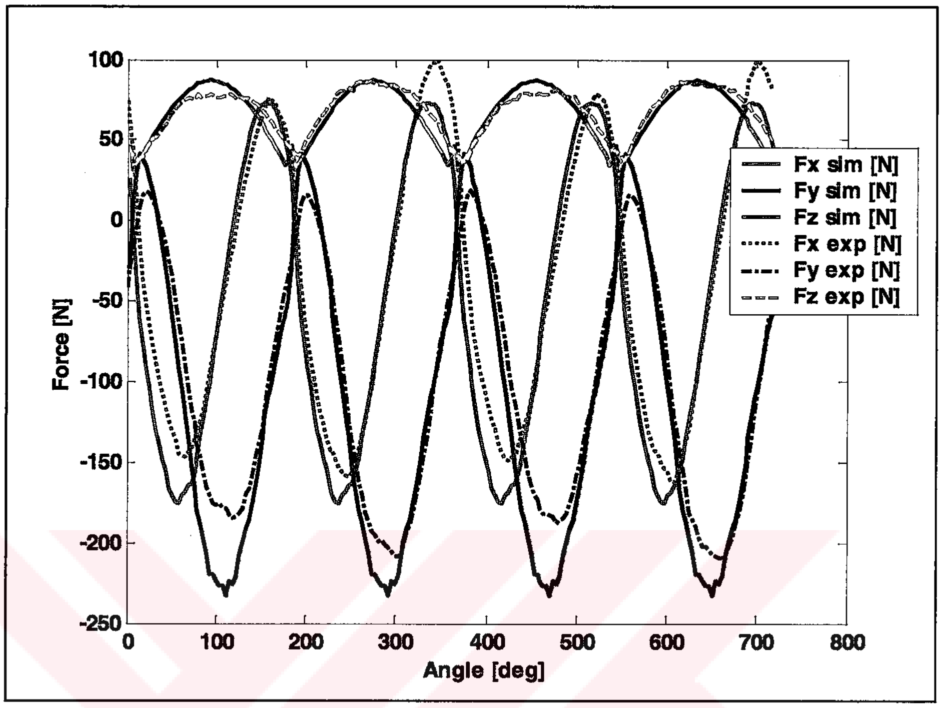

b) 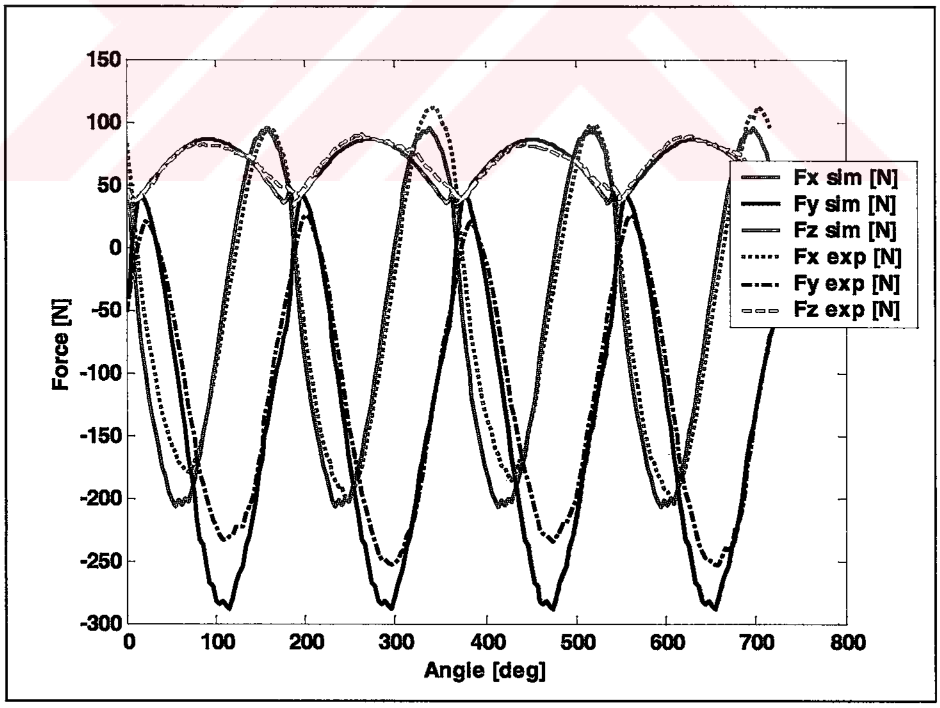

Figure 5.5: Predicted and measured forces vs. angular advance for;
a) 3 mm depth of cut b) 4 mm depth of cut

a)

b)

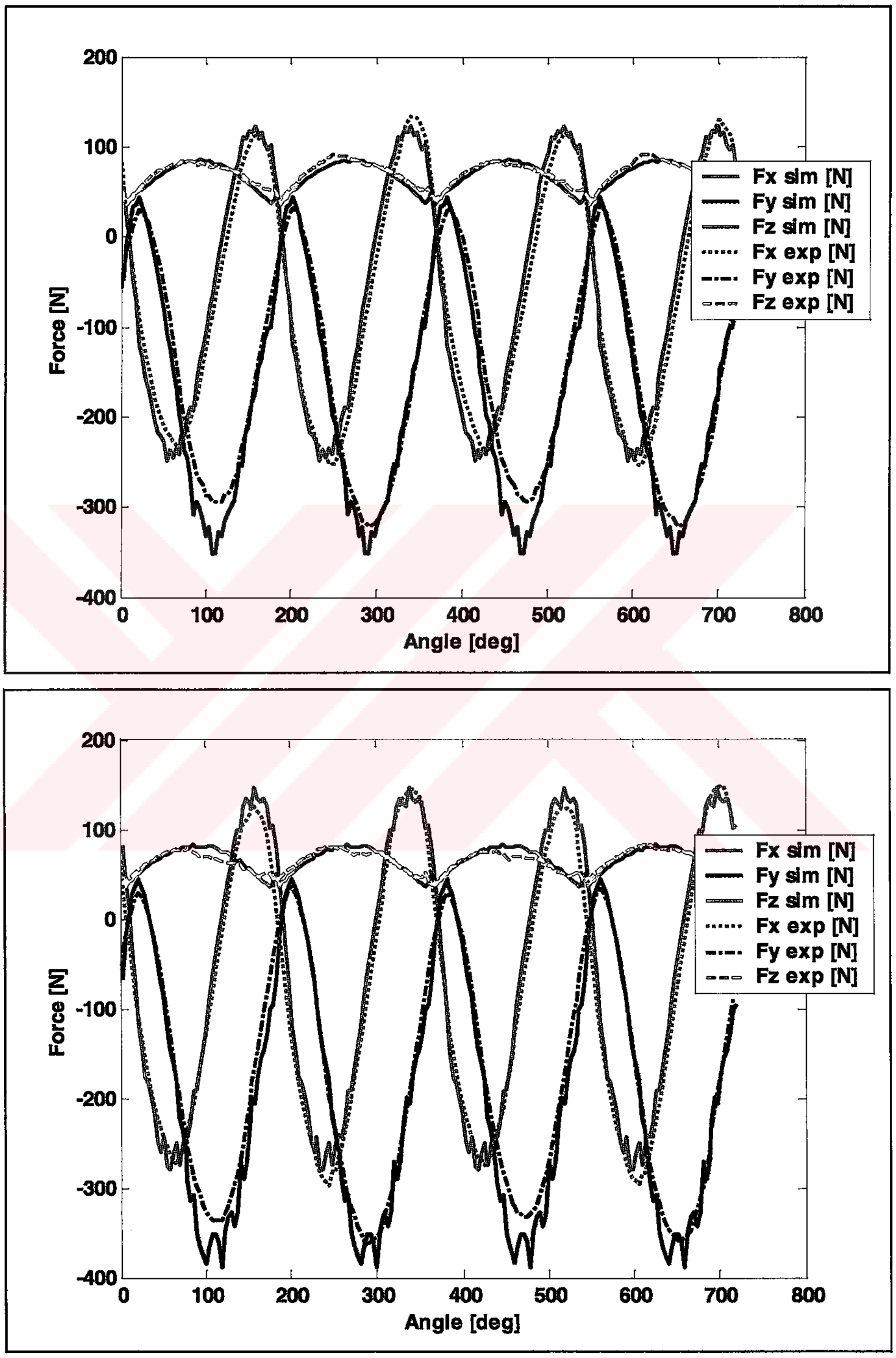

Figure 5.6: Predicted and measured forces vs. angular advance for;
a) 5 mm depth of cut b) 6 mm depth of cut

5.2.2 Half immersion cut

Cuts other than slot cutting can be grouped as up milling and down milling cases in 2½ axis milling. In the up milling process, the chip thickness varies from zero to maximum. In down milling, the chip thickness starts from the maximum and decreases to zero at exit. Down milling usually produces better surface finish since the shearing process ends at the finished surface.

Normally different coding of the model algorithm is required for up milling and down milling cases. But the simulation model proposed in this study is a generic one in the sense that it predicts the cutting forces for different cases without making any changes.

The results of predictions for up and down milling cases have been investigated next. Two straight half immersion paths have been cut for up and down milling. Cutting conditions are summarized in Table 5.2. The simulation outputs for these have been given in Figure 5.7 with the engagement regions during cut. Predicted and measured forces are given in Figure 5.8. Again the predicted results show good agreement with reality.

Table 5.2 Cutting conditions for half immersion slot cuts

Test no.	9 - 10
Feed rate	48 mm/min
Depth of cut	6 mm
Spindle Speed	600 rpm
Amplifier gain	100
Sampling frequency	1000
Sampling time	1 s
Tool path	20 mm straight, horizontal in x direction, tip moving along workpiece right/left edge for up/down milling

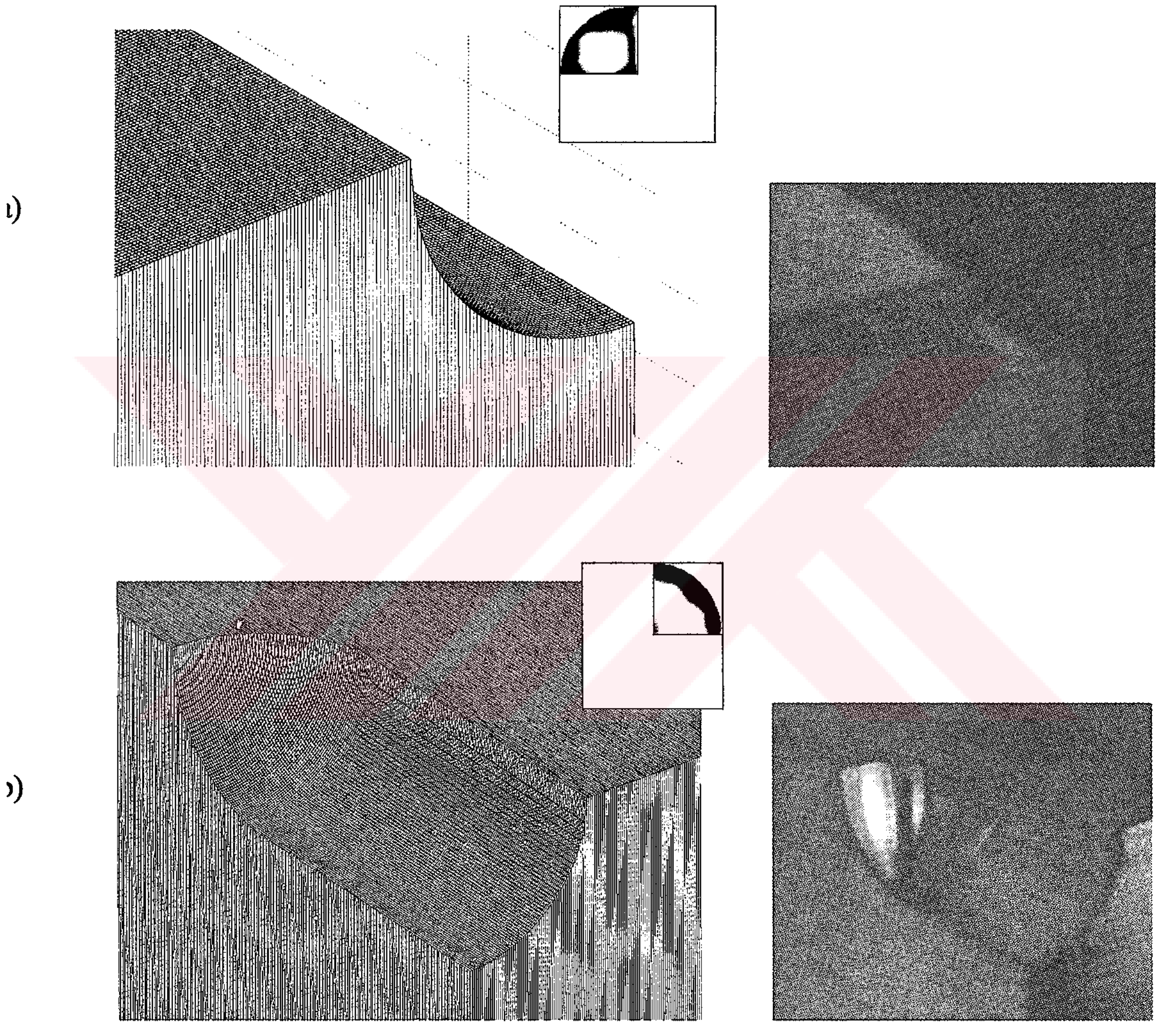

Figure 5.7: Simulation outputs and related engagement regions for 6 mm depth of cut. vs actual cut; a) up milling, b) down milling.

a)

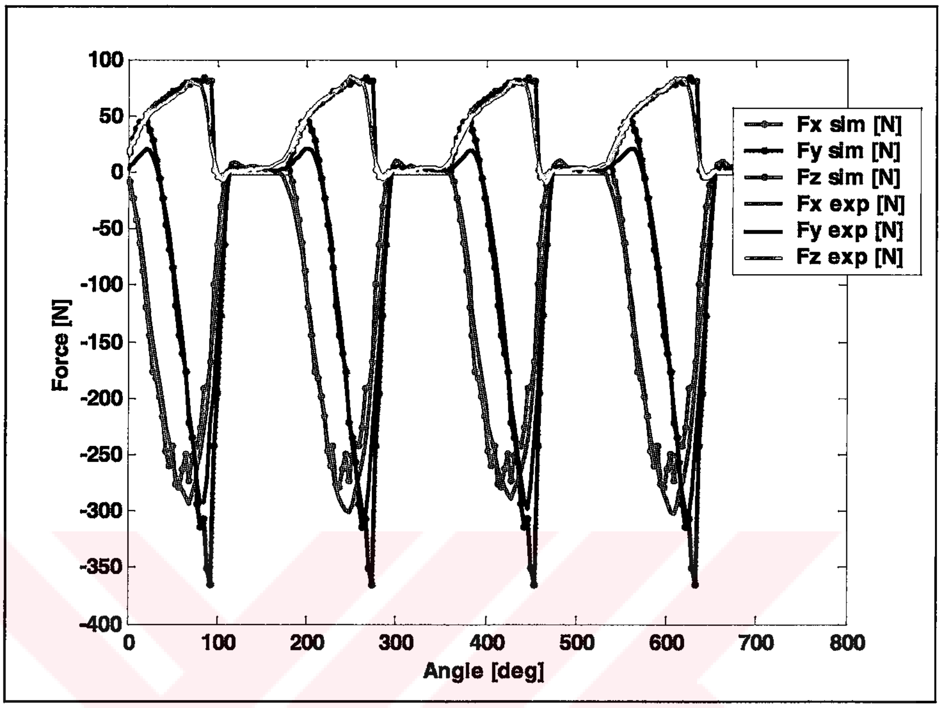

b)

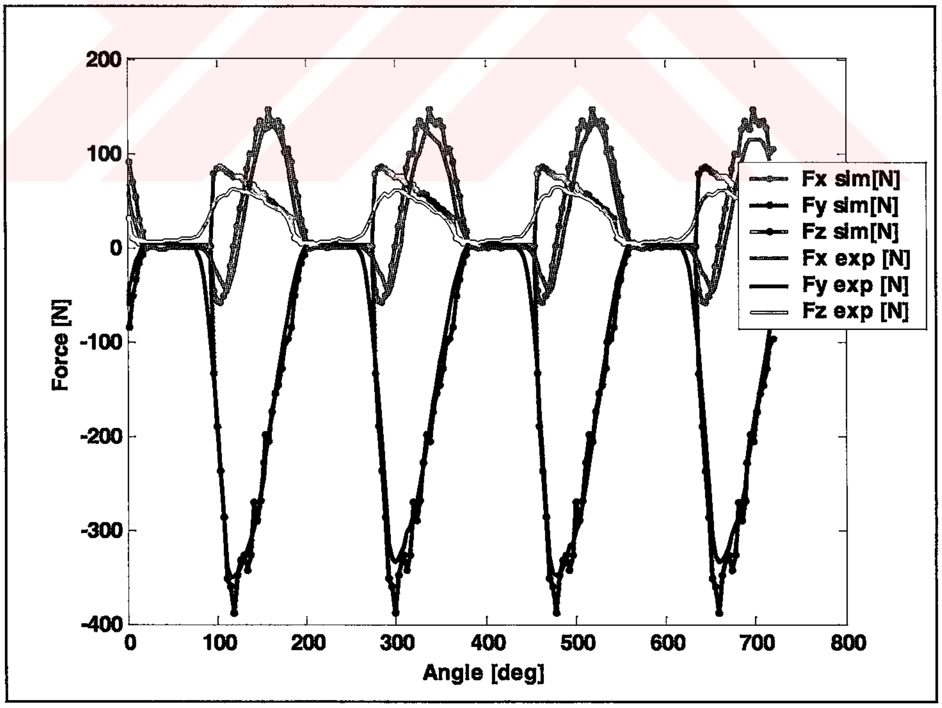

Figure 5.8: Predicted and measured forces vs. angular advance for 6 mm depth of cut and 48 mm/min feed; a) up milling, b) down milling.

5.2.3 Bisectional cut

A more complex type of 2½ milling case has been tested. The performance of the force model in case of a bisectional engagement region has been investigated.

Initially the workpiece has been step-cut using a straight-end mill. Steps of 5 mm width and height have been obtained. Thereafter the cutter has been positioned in one of the steps so that the depth of cut will be maximum 1 mm from both dimensions during cut. Cutting conditions are summarized in Table 5.3. As seen in Figure 5.9 the engagement region obtained is bisectional as well. Predicted and measured forces are given in Figure 5.10. The model over-predicted the experimental results for the forces in *x* and *z* directions. But the predicted force pattern showed good agreement with the actual one.

Table 5.3 Cutting conditions for bisectional cut

Test no.	11
Feed rate	48 mm/min
Depth of cut	1 mm
Spindle Speed	600 rpm
Amplifier gain	100
Sampling frequency	1000
Sampling time	1 s
Tool path	20 mm straight, horizontal in x direction, tip moving along edge of 5 mm high and 5mm wide step.

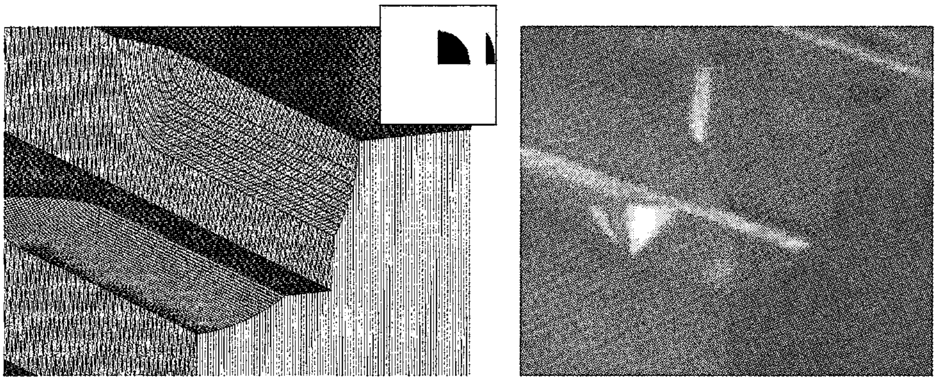

Figure 5.9: Simulation output and the engagement region vs. actual cut for bisectional cut.

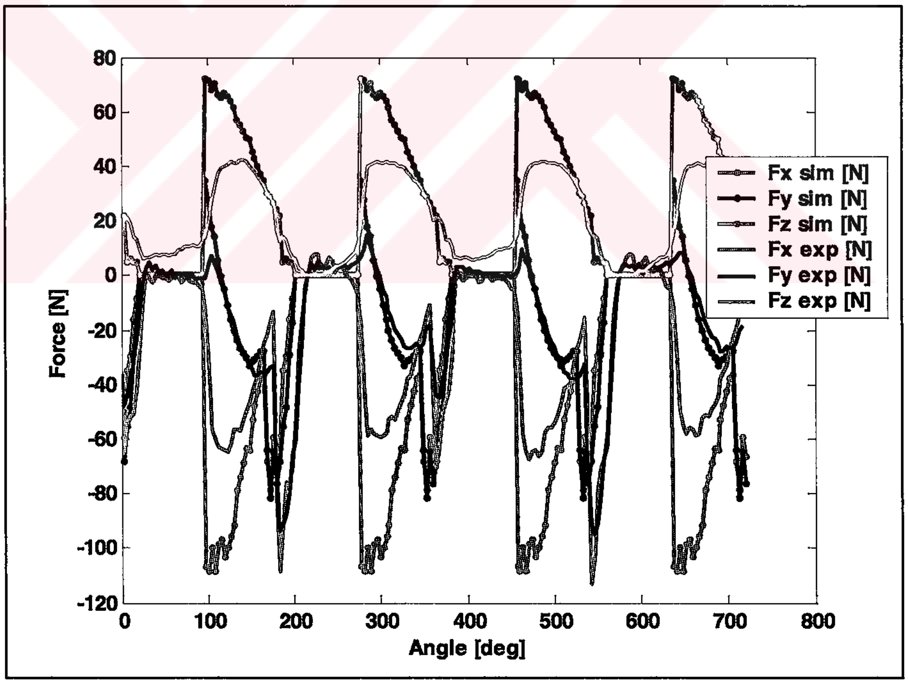

Figure 5.10: Predicted and measured forces vs. angular advance for bisectional cut.

5.3 Sculpture Surface Tests

After obtaining satisfactory prediction results in the 2½ milling case, the model has been tested for sculpture or namely 'free form' surfaces. Several tests have been performed including the basic free forms, convex and concave cuts. As a complicated assignment, the model has also been tested for a cross-step cut.

5.3.1 Convex Cut

The cutter has been moved through a convex path into the workpiece. Cutting conditions are summarized in Table 5.4. The simulation output for convex cut has been given in Figure 5.11. Measured forces and predictions made by simulation for convex cut are given in Figure 5.12. The model over-predicted the force in vertical direction. The under-prediction for x and y forces can be partly explained by the runout in actual cuts but predicted force patterns showed fairly good agreement with the actual patterns.

Table 5.4 Cutting conditions for convex cut

Test no.	12
Feed rate	48 mm/min
Depth of cut	Up to 6 mm
Spindle Speed	600 rpm
Amplifier gain	100
Sampling frequency	1000
Sampling time	80 s
Tool path	32.29 mm curved through convex arc of 25 mm radius in x-z plane

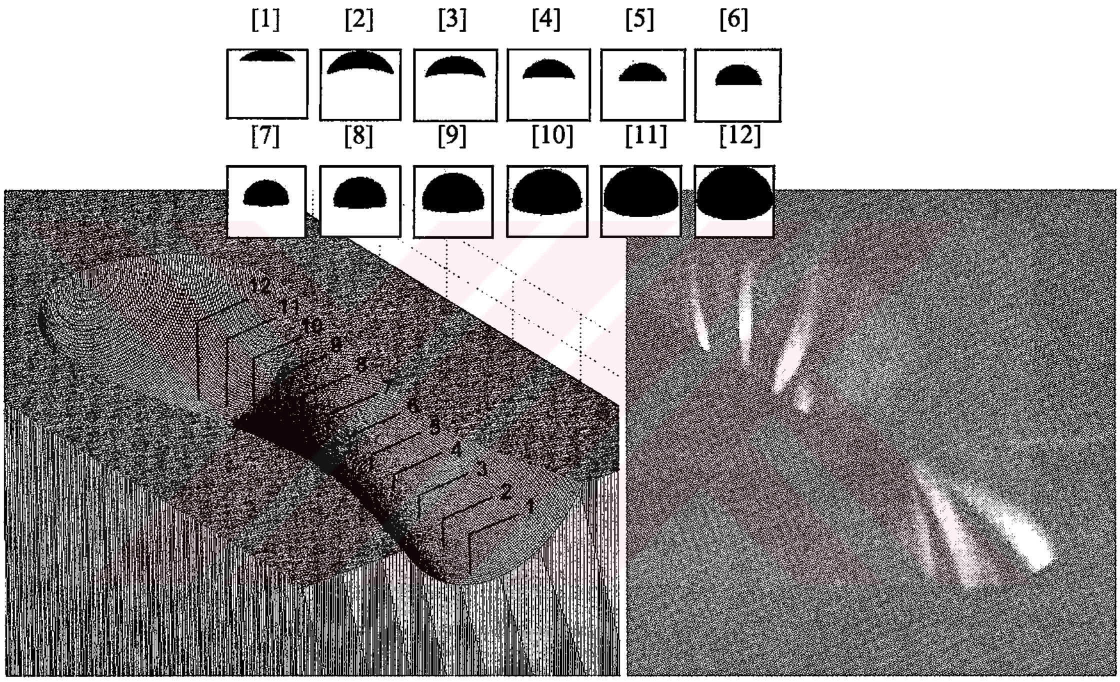

Figure 5.11: Simulation output and the engagement regions vs. actual cut for convex cut.

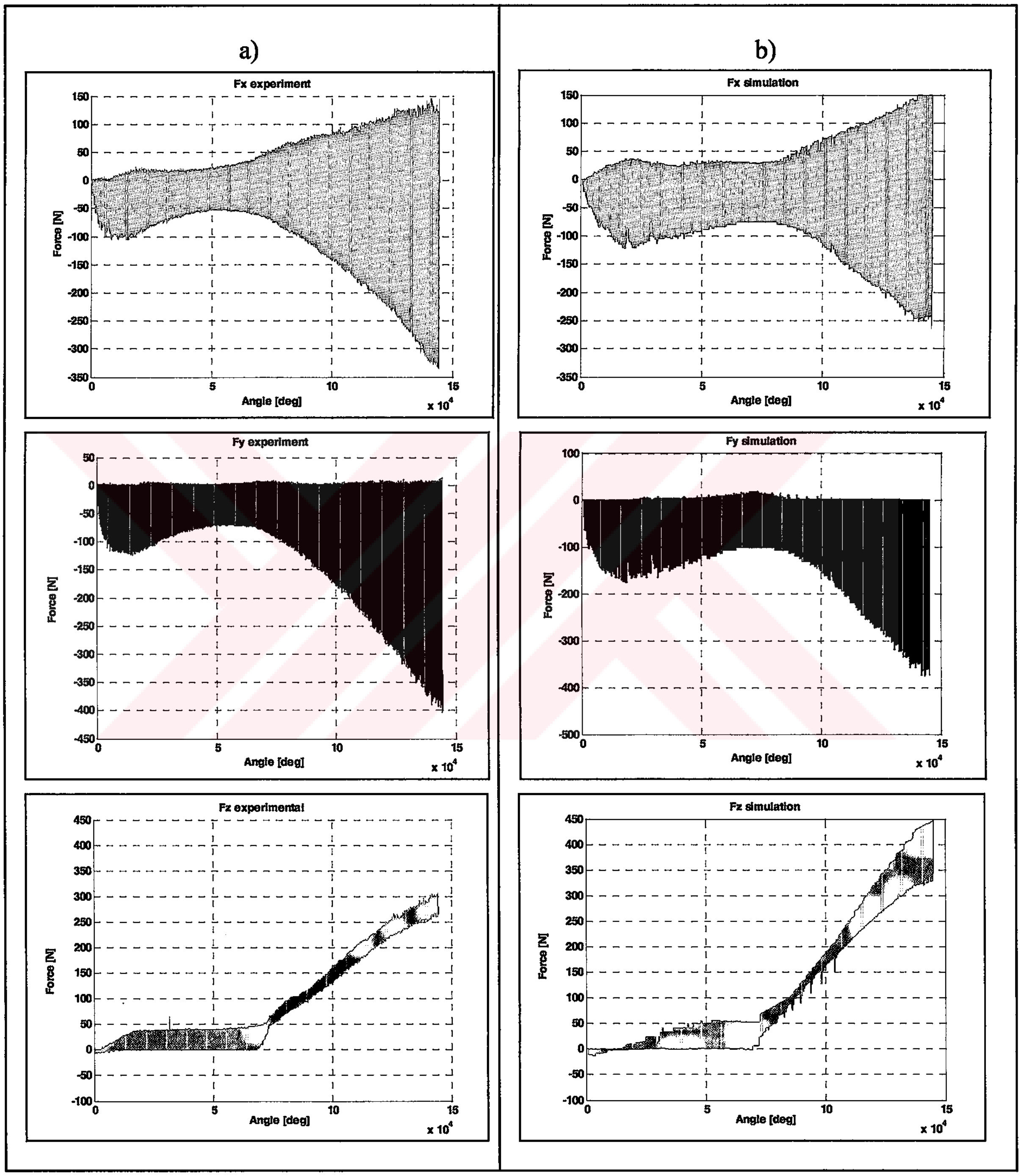

Figure 5.12: a) Measured cutting forces, b) Forces predicted by model

5.3.2 Concave Cut

The cutter has been moved through a concave path in the x-z plane this time. Cutting conditions are summarized in Table 5.5. The simulation output for concave cut has been given in Figure 5.13. Measured forces and predictions made by simulation for concave cut are given in Figure 5.14. The force in vertical direction has been successfully predicted. The under-prediction in prediction of x and y forces can again be explained by runout in the cutter. Because when one flute cuts more than the average chip load, observed maximum for the cutting forces is naturally higher than expected. Force pattern predictions, again, showed good agreement with the actual patterns.

Table 5.5 Cutting conditions for concave cut

Test no.	13
Feed rate	48 mm/min
Depth of cut	Up to 4 mm
Spindle Speed	600 rpm
Amplifier gain	100
Sampling frequency	1000
Sampling time	60 s
Tool path	17.89 mm curved through concave arc of 12 mm radius in x-z plane

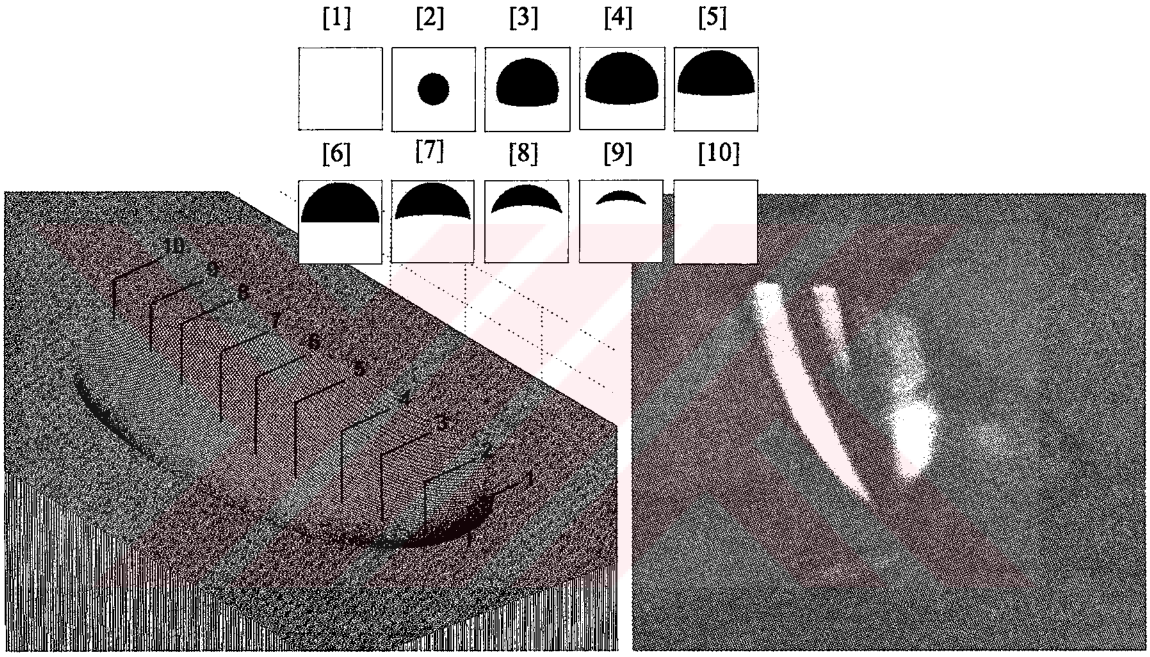

Figure 5.13: Simulation output and the engagement regions vs. actual cut for concave cut.

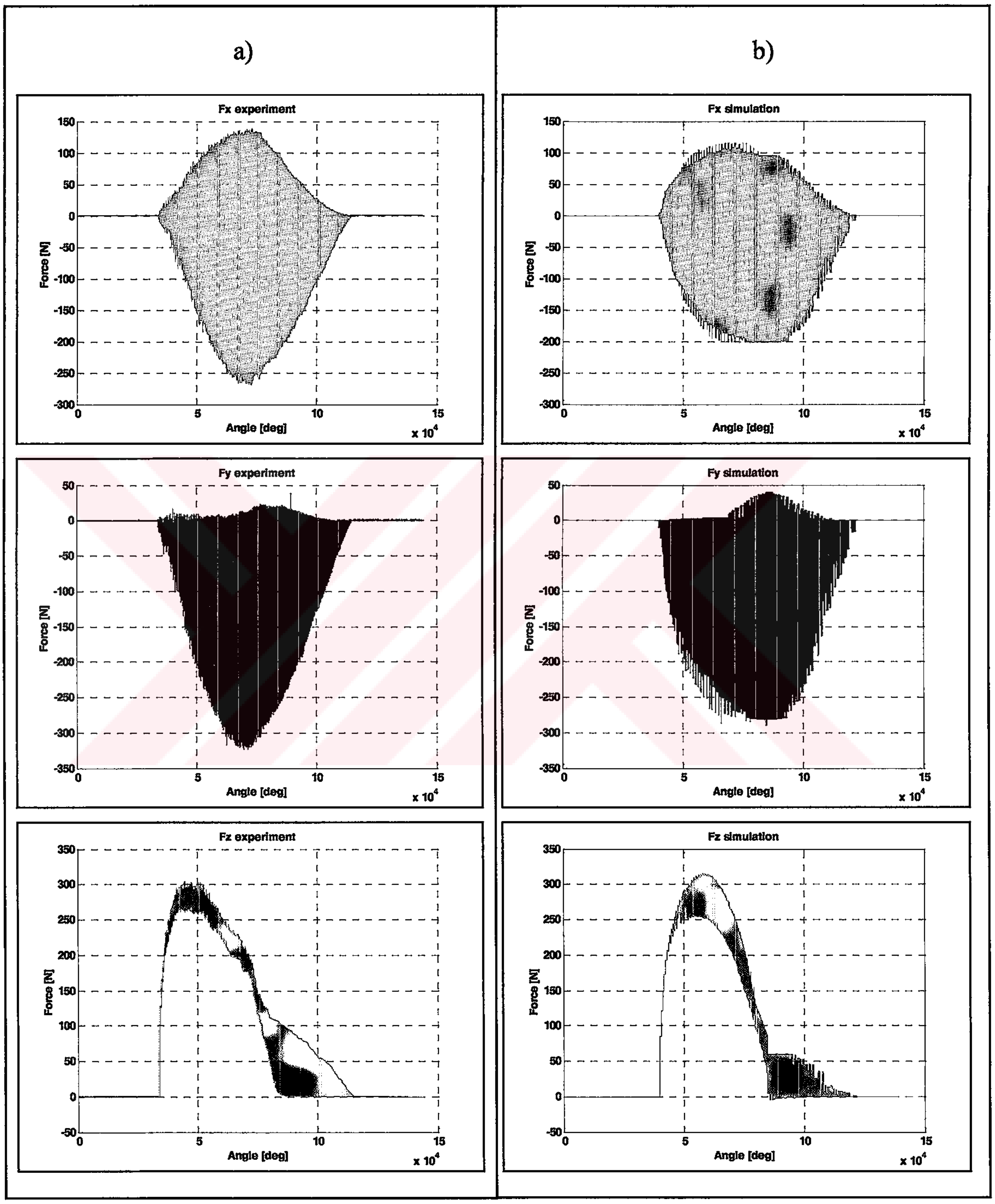

Figure 5.14: a) Measured cutting forces, b) Forces predicted by model

5.3.3 Cross-Step Cut

A complicated cut which would imitate the semi-finishing or the finishing process in actual cutting operations has been tested this time. Usually a rough cut is followed by semi-finishing and/or finishing in order to complete the milling process in manufacturing. Considering this fact, 5 mm high and wide step cuts has been cut using a straight-end mill in this test. Thereafter a linear cross-cut has been made with the ball end mill through the initially cut steps.

Cutting conditions for this test are summarized in Table 5.6. The simulation output for cross-step cut has been given in Figure 5.15. Measured forces and predictions made by simulation for the cut are in Figure 5.16. There was considerable runout in the cutter for this test which again led to under-estimations in force predictions at various levels. On the other hand, the positive components of the force in x direction have been over-predicted through the path. However, predicted force patterns matched that of the actual ones.

Table 5.6 Cutting conditions for cross-step cut

Test no.	14
Feed rate	48 mm/min
Depth of cut	Up to 4 mm
Spindle Speed	600 rpm
Amplifier gain	100
Sampling frequency	1000
Sampling time	35 s
Tool path	25.46 mm linear, 45° down the x direction in *x-z* plane

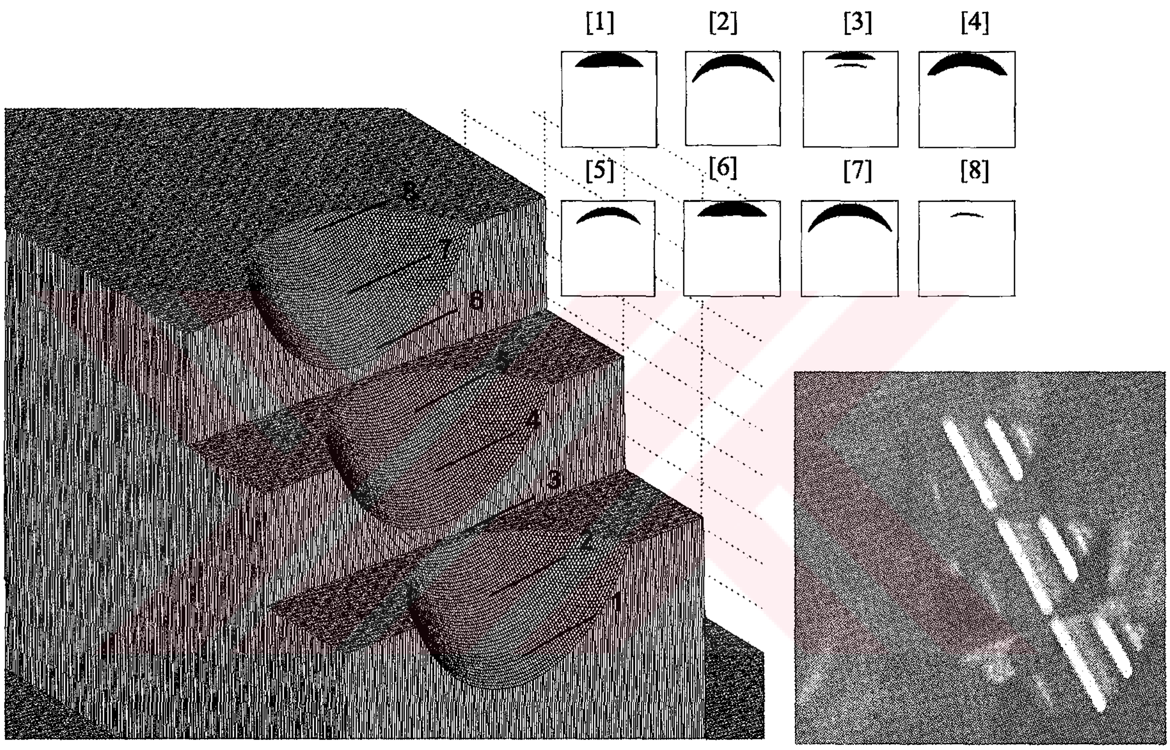

Figure 5.15: Simulation output and the engagement regions vs. actual cut for cross-step cut.

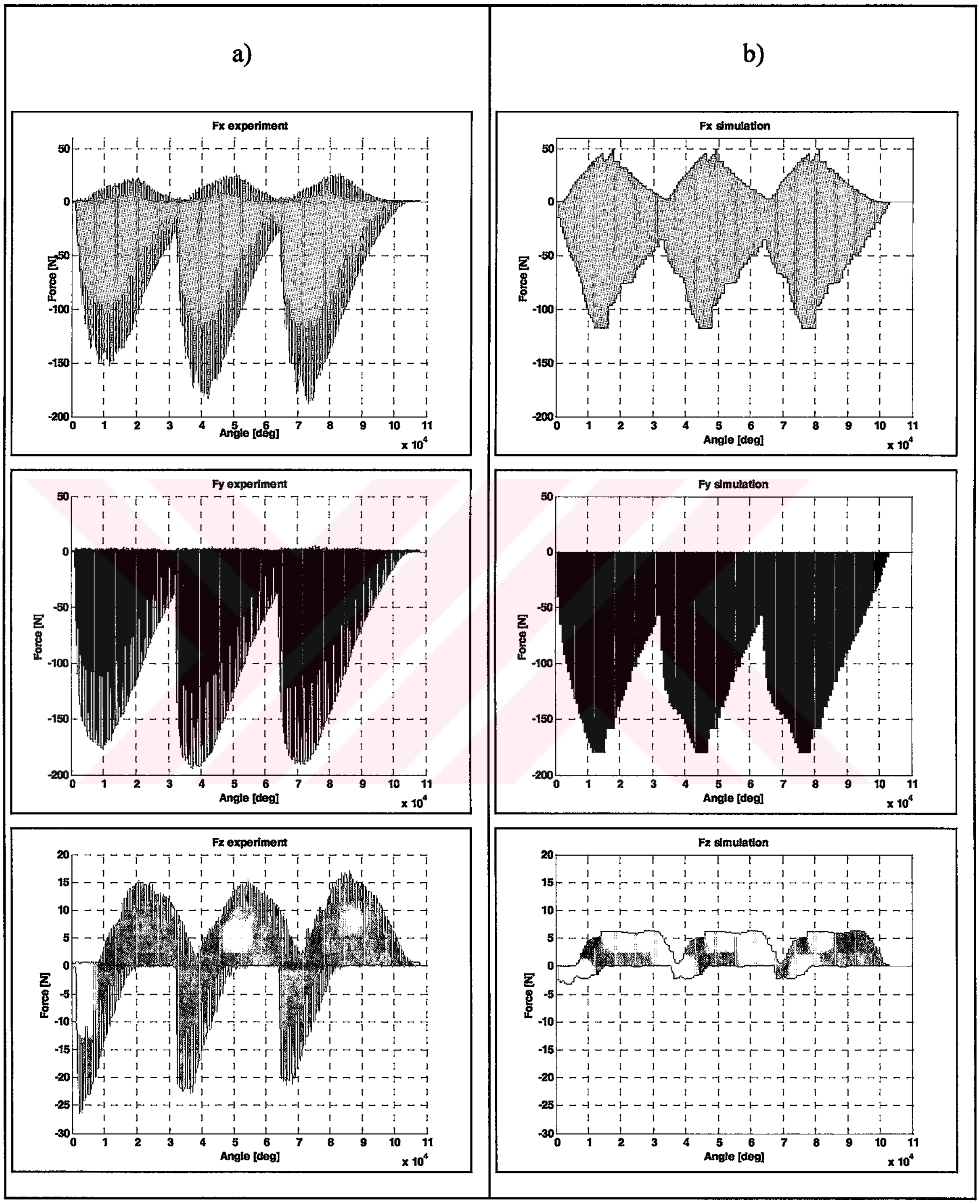

Figure 5.16: a) Measured cutting forces, b) Forces predicted by model

5.4 Surface Topography Validation

Other than testing and validating the prediction of cutting forces, a sample surface has been selected to validate the prediction of surface topography and scallop height variations. The machined concave surface has been measured using a coordinate measurement machine for comparison (Figure 5.17).

Brown & Sharpe/Dea Scirocco CMM with Ø 2 mm sensor tip has been used for measurement of the surface point coordinates. Data points have been gathered through a meshed grid of mesh size 0.1 mm x 0.5 mm (Figure 5.18.a). The obtained simulation output for the concave surface had 0.1 mm x 0.1 mm mesh size (Figure 5.18.b). The height values of the corresponding points of the simulation output and the CMM measurement have been subtracted in order to obtain the prediction error related to surface topography (Figure 5.19.a).

There was a substantial difference between prediction and reality near the sides of the cut which was due to the roughness in measurements using Ø 2 mm CMM sensor tip. The tip was insufficient for precisely measuring sharp edges. Therefore a comparison excluding the side edges has been made in Figure 5.19.b. Here again the upper and lower edges of the viewed cut is not accurately measured by CMM where the prediction error is around 300 μm. However, if these edges are ignored it is seen that the accuracy of surface topography predictions are around 200 μm and less.

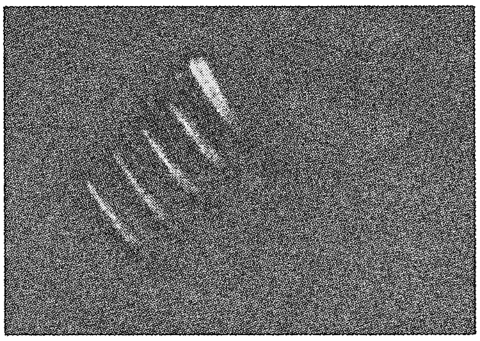

Figure 5.17: The concave surface machined for the test.

a)

b)

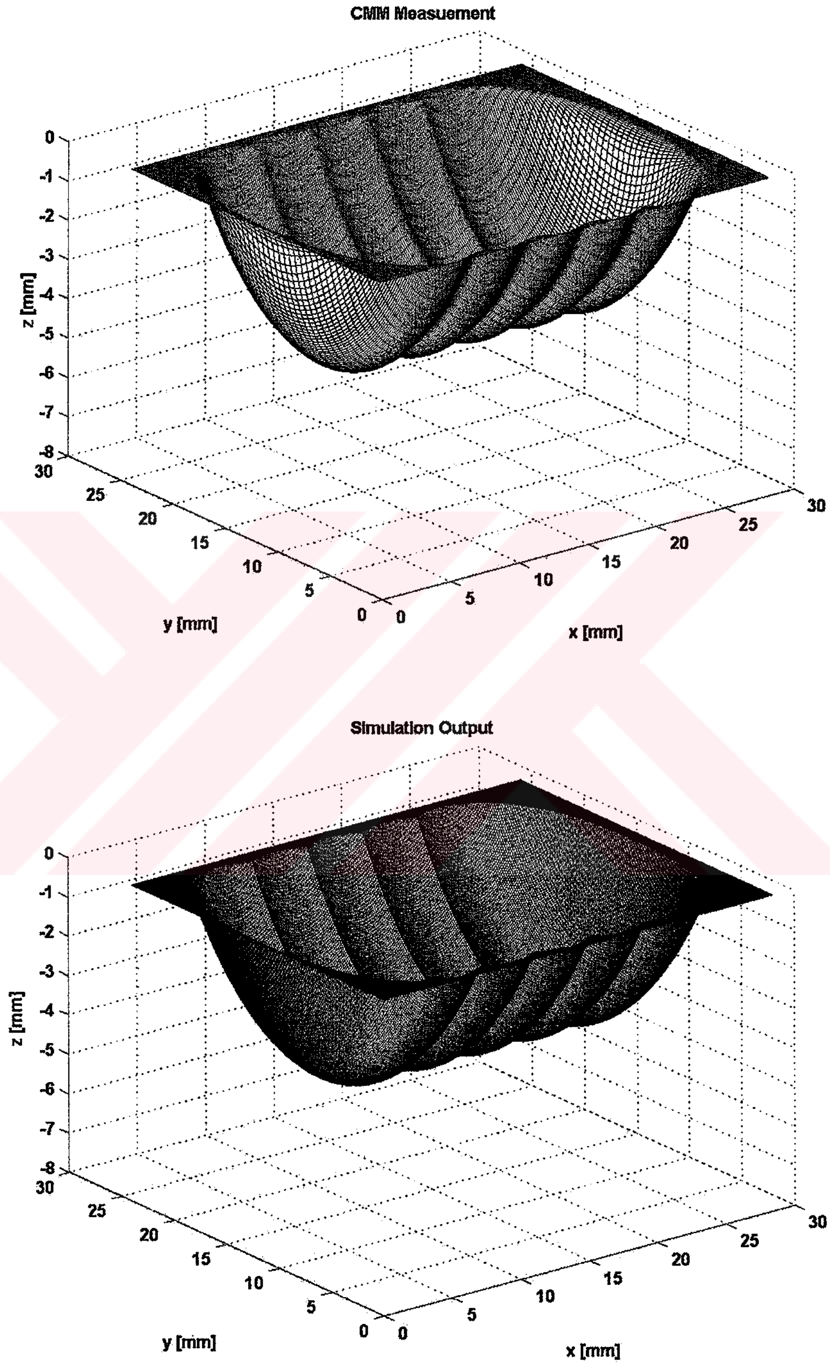

Figure 5.18: a) Data points obtained by CMM, b) Simulation output for the machined surface

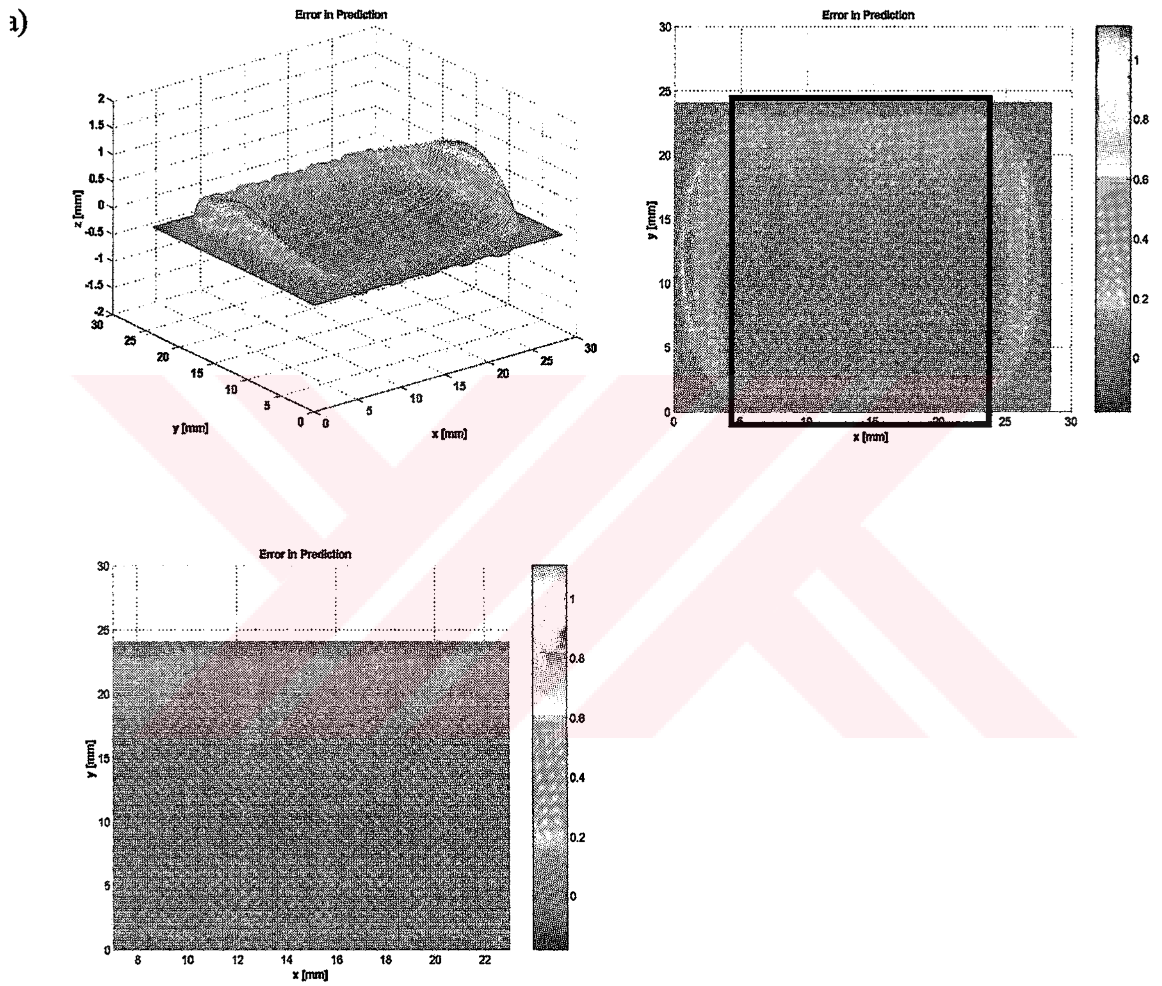

Figure 5.19: a) Prediction error on the overall surface, b) Prediction error excluding the sides

Chapter 6

CONCLUSION

The objective of the thesis has been to develop a practical method to predict the behavior of ball-end milling operations. Special emphasis has been placed on the prediction of cutting forces in sculpture surface machining operations which are widely used in machining dies, molds, automobile and aerospace parts. The results of this study provide the prediction of the direction and amplitude of cutting forces applied on the cutter and workpiece structures together with the prediction of resulting surface topography and scallop height variations. The prediction of cutting forces in advance helps the process engineers to select 'appropriate values' for the process parameters to achieve a more productive machining level. Besides, knowledge on the cutting forces helps to design better fixtures, contributing to an increase in surface qualities of parts.

In this study, the tool geometry of the ball-end mill has been defined in Cartesian coordinates initially. The ball-end mill cutter and the workpiece have been modeled using Matlab in order to obtain a mathematical frame that will be utilized by the force model. Mesh structures have been employed to represent the cutter and workpiece in mathematical domain. The engagement regions during cut have been detected by the model algorithm through use of a Boolean approach. Models in previous studies commonly did not detect the engagement regions under complicated cutting conditions whereas the proposed model adequately detects the contact region for even the most complicated cuts. Accurate prediction of engagement regions is the basis for making reliable predictions using a force model. The surface topography predictions made by the developed cutter/workpiece intersection model also agreed well with the CMM measurements.

The engagement region predictions were the inputs of the force model together with the cutting and edge constants. Whereas the previous models usually employed transformation methods to make use of orthogonal cutting constants, in this study, the cutting constants have been directly calculated using a practical calibration method. Cutting forces have been analyzed for different regions of the cutter during slot cutting tests and it is seen that these forces have a linear behavior for changing feed rate at each region. As a result cutting and edge constants have been derived through use of the linear relationship between feed rate and cutting forces. The cutting constants had substantially high values near the tip of the cutter and stabilized to certain values as the distance from tip was increased.

Most of the previous ball-end milling models do not take into consideration the forces in vertical direction for sculpture surface machining. In order to accomplish this, a constant pressure that contributes to the vertical cutting force is analyzed in this work. An equation has been obtained for this pressure value for changing feed rate. Later, the obtained pressure value has been multiplied with the contact area of the ball-end mill cutter for all instants of the simulation in order to obtain the contribution to force in vertical direction at any instant.

By the time all inputs for the force model to function have been provided, validation tests have been made in order to test the system. All tests have been realized in the 12 mm/min-48 mm/min feed rate interval since the performed calibration covered this interval. Slot cutting, up and down milling and a bisectional cut have been tested as 2½ axis milling cases. There has been considerable runout in the tests with smaller feed rates, but for feed rates near 48 mm/min quite accurate predictions have been obtained for the cutting forces. Force predictions for both convex, concave surfaces have been tested as sculpture surface machining cases. Additionally a cross-step cut has been tested where step cuts represent the rough cuts and the cross cuts using a ball-end mill represent the fine cuts in an actual manufacturing process. Predicted and measured forces showed good agreement in the performed sculpture surface tests as well.

Possible enhancements to this model will be including the effect of cutter runout and form errors due to deflection of the cutter. More accurate results will be obtained for even extreme, undesirable cutting conditions once these additions are provided to the model.

The model that is developed in this study is supposed to directly contribute to increasing the productivity of a manufacturing system through feed rate optimization. Once a limiting peak force is defined for the cutter (by the manufacturer of the cutter or a process engineer that has experienced the cutter), the model will give a pattern for the changing cutting forces during a manufacturing operation and indicate the regions where feed rate can be increased, thus substantially decreasing the production time for sculpture surfaces where depth of cut and cutting forces are continuously changing.

BIBLIOGRAPHY

[1] Y. Altintas, Manufacturing Automation: Metal Cutting Mechanics, Machine Tool Vibrations, and CNC Design, Cambridge University Press, (2000).

[2] M. Yang and H. Park, The Prediction of Cutting Force in Ball-End Milling, Int. J. Mach. Tools Manufact., 31 (1991), 45-54.

[3] I. Lazoglu, Sculpture Surface Machining: A Generalized Model of Ball-End Milling Force System, International Journal of Machine Tools & Manufacture, 43 (2003), 453-462.

[4] P. Lee, Mechanics and Dynamics of Ball-End Milling, M. Sc. thesis, University of British Columbia, (1995).

[5] M.E. Martelotti, An Analysis of the Milling Process, Transactions of the ASME, 63 (1941), 677-700.

[6] F. Koenigsberger, A.J.P. Sabberwal, An Investigation into the Cutting Force Pulsations During Milling Operations, International Journal of Machine Tool Design and Research, 1 (1961), 15-33.

[7] W.A. Kline, R.E. DeVor, and I.A. Shareef, The Effect of Runout on Cutting Geometry and Forces in End Milling, International Journal of Machine Tools Design and Research, 23 (1983), 123-140.

[8] H.J. Fu, A Dynamic Modeling Approach to the Optimal Design of Nonuniform Chip Loading in Face Milling, Ph.D. thesis, University of Illinois, 1985.

[9] J. Tlusty and P. MacNeil, Dynamics of Cutting Forces in End Milling, Annals of the CIRP, 24 (1975), 21-25.

[10] E.J.A. Armarego and N.P. Deshpande, Force Prediction Models and CAD/CAM Software for Helical Tooth Milling Processes, I, Basic approach and Cutting Analyses, International Journal of Production Research 31 (1993), 1991-2009.

[11] E.M. Lim, H.Y. Feng, C.H. Menq, The Prediction of Dimensional Errors for Machining Sculptured Surfaces Using Ball-End Milling, in K.F. Ehmann, editor, Manufacturing Science and Engineering, 149-156. ASME Winter Annual Meeting, New Orleans, USA, 1993, PED-Vol.64.

[12] E.M. Lim, H.Y. Feng, C.H. Menq, Z. H. Lin, The Prediction of Dimensional Error for Sculptured Surface Productions Using the Ball-End Milling Process, I, Chip Geometry Analysis and Cutting Force Prediction, Int. J. Mach. Tools Manufact., 35 (1995), 1149-1169.

[13] G. Yucesan and Y. Altintas, Mechanics of Ball End Milling Process, in K.F. Ehmann, editor, Manufacturing Science and Engineering, 543-551. ASME Winter Annual Meeting, New Orleans, USA, 1993, PED-Vol.64.

[14] E.J.A. Armarego and R.C. Whitfield, Computerized End-Milling Force Predictions with Cutting Models Allowing Eccentricity and Cutter Deflections, Annals of the CIRP, 40 (1991), 25-29.

[15] E. Budak, Y. Altintas, and E.J.A. Armarego, Prediction of Milling Force Components from Orthogonal Cutting Data.

[16] M. Yang and H. Park, The Prediction of Cutting Force in Ball-End Milling, Int. J. Mach. Tools Manufact., 31 (1991), 45-54.

[17] K. H. Tai, C.C. Fuh, A Predictive Force Model in Ball-End Milling including Eccentricity Effects, International Journal of Machine Tool Design and Research, 34 (1994), 959-979.

[18] I. Lazoglu, S.Y. Liang, Modeling of Ball-End Milling Forces with Cutter Axis Inclination, Journal of Manufacturing Science and Engineering, Transactions of the ASME 122 (2000), 3-11.

[19] S.A. Tobias and W. Fishwick, The Chatter of Lathe Tools under Orthogonal Cutting Conditions, Transactions of the ASME, 80 (1958), 1079-1088.

[20] J. Tlusty and M. Polacek, The Stability of Machine Tools Against Self Excited Vibrations in Machining, International Research in Production Engineering, ASME, (1963) 465-474.

[21] R. Sridhar, R.E. Hohn, and G.W. Long, General Formulation of the Milling Process Equation, Trans. ASME Journal of Engineering for Industry, (1968) 317-324.

[22] I. Minis and T. Yanushevsky, A New Theoretical Approach for the Prediction of Machine Tool Chatter in Milling, Trans. ASME Journal of Engineering for Industry, 115 (1993), 1-8.

[23] E. Budak, Mechanics and Dynamics of Milling with Flexible Structures, PhD thesis, University of British Columbia, October 1994.

[24] Y. Altintas, P. Lee, Mechanics and Dynamics of Ball-End Milling, ASME Journal of Manufacturing Science and Engineering, 120 (1998), 684-692.

[25] F. Abrari, M.A. Elbestawi, A.D. Spence, On the Dynamics of Ball End Milling: Modeling of Cutting Forces and Stability Analysis, Int. J. Mach. Tools Manufact., 38 (1998), 215-237.

[26] G.M. Kim, P.J. Cho, C.N. Chu, Cutting Force Prediction of Sculptured Surface Ball-End Milling Using Z-Map, International Journal of Machine Tools & Manufacture, 40 (2000), 277-291.

[27] G.M. Kim, B.H. Kim, C.N. Chu, Estimation of Cutter Deflection and Form Error in Ball-End Milling Processes, International Journal of Machine Tools & Manufacture, 43 (2003), 917-924.

[28] B.W. Ikua, H. Tanaka, F. Obata, S. Sakamoto, Prediction of Cutting Forces and Machining Error in Ball-end Milling of Curved Surfaces, I, Theoretical Analysis, Journal of the International Societies for Precision Engineering and Nanotechnology, 25 (2001), 266-273.

[29] B.W. Ikua, H. Tanaka, F. Obata, S. Sakamoto, T. Kishi, T. Ishii, Prediction of Cutting Forces and Machining Error in Ball-end Milling of Curved Surfaces, II, Experimental Verification, Journal of the International Societies for Precision Engineering and Nanotechnology, 26 (2002), 69-82.

[30] Y.H. Jung, J.S. Kim, S.M. Hwang, Chip Load Prediction in Ball-End Milling, Journal of Materials Processing Technology, 111 (2001), 250-255.

[31] M. Shatla, T. Altan, Analytical Modeling of Drilling and Ball-End Milling, J. Mat. Proc. Tech., 98 (2000), 125-133.

[32] K.-D. Bouzakis, P. Aichouh, K. Efstathiou, Determination of the Chip Geometry, Cutting Force and Roughness in Free Form Surfaces Finish Milling with Ball End Tools, Int. J. Mach. Tools & Manuf., 43 (2003), 499-514.

VITA

Birhan Ufku Guzel completed the high school in Izmir Fen Lisesi, Izmir, in 1997. He received his B. Sc. degree in Industrial Engineering from Bogazici University (BU), Istanbul, in 2001. As his graduation project he has been involved in a departmental project in B.U. dealing with Automated Guided Vehicles (AGVs). The project consisted of building an object oriented test-bed for AGV systems, thereby forming a simulation environment for searching out optimal conditions in a material handling system using AGVs in a flexible manufacturing environment. Since 2001 he is in the M. Sc. program in Industrial Engineering of Koc University as a teaching/research assistant. For the completion of the program he has taken part in a mechanical engineering project with the title 'Sculpture Surface Machining'.